On the seasonal variability of the Canary Current and the Atlantic Meridional Overturning Circulation

Pedro Vélez-Belchí[1] (iD), **M. Dolores Pérez-Hernández[2,3]** (iD), **María Casanova-Masjoan[2]** (iD), **Luis Cana[2]** (iD)**, and Alonso Hernández-Guerra[2]** (iD)

[1]Centro Oceanográfico de Canarias, Instituto Español de Oceanografía, Santa Cruz de Tenerife, Canary Islands, Spain, [2]Instituto de Oceanografía y Cambio Global, Universidad de Las Palmas de Gran Canaria, Canary Islands, Spain, [3]Now at Department of Physical Oceanography, Woods Hole Oceanographic Institution, Woods Hole, Massachusetts, USA

Abstract The Atlantic Meridional Overturning Circulation (AMOC) is continually monitored along 26°N by the RAPID-MOCHA array. Measurements from this array show a 6.7 Sv seasonal cycle for the AMOC, with a 5.9 Sv contribution from the upper mid-ocean. Recent studies argue that the dynamics of the eastern Atlantic is the main driver for this seasonal cycle; specifically, Rossby waves excited south of the Canary Islands. Using inverse modeling, hydrographic, mooring, and altimetry data, we describe the seasonal cycle of the ocean mass transport around the Canary Islands and at the eastern boundary, under the influence of the African slope, where eastern component of the RAPID-MOCHA array is situated. We find a seasonal cycle of -4.1 ± 0.5 Sv for the oceanic region of the Canary Current, and $+3.7 \pm 0.4$ Sv at the eastern boundary. This seasonal cycle along the eastern boundary is in agreement with the seasonal cycle of the AMOC that requires the lowest contribution to the transport in the upper mid-ocean to occur in fall. However, we demonstrate that the linear Rossby wave model used previously to explain the seasonal cycle of the AMOC is not robust, since it is extremely sensitive to the choice of the zonal range of the wind stress curl and produces the same results with a Rossby wave speed of zero. We demonstrate that the seasonal cycle of the eastern boundary is due to the recirculation of the Canary Current and to the seasonal cycle of the poleward flow that characterizes the eastern boundaries of the oceans.

1. Introduction

The Atlantic Meridional Overturning Circulation (AMOC) is an important component of the climate system since it makes the largest oceanic contribution to the meridional transport of heat [*Ganachaud*, 2003]. Due to its importance, the strength of the AMOC is continually monitored along 26.5°N by several moorings grouped in three sets according to their location: east of the Bahamas, at the Mid-Atlantic Ridge, and over the African slope south of the Canary Islands [*McCarthy et al.*, 2015]. This ocean observing system is known as U.K.-U.S. Rapid Climate Change-Meridional Overturning Circulation and Heatflux Array (hereafter the RAPID-MOCHA array) and its data have changed our understanding of the AMOC [*Cunningham et al.*, 2007; *Kanzow et al.*, 2007]. Among others, it changed the previous paradigm where the seasonal anomalies of the AMOC were dominated by fluctuations of the Ekman transport [*Bryan*, 1982; *Böning et al.*, 1994; *Jayne and Marotzke*, 2001]. *Chidichimo et al.* [2010] found, with the first 4 years of data, a peak-to-peak seasonal cycle of the AMOC of 6.7 Sv, and attributed 5.2 Sv of this seasonal cycle to the eastern boundary. *Kanzow et al.* [2010] corroborated the results and showed that the mean strength of the AMOC is 18.7 Sv northward, with the maximum in fall and the minimum in spring. From the three main components of the AMOC at 26.5°N, that is Gulf Stream (T_{GS}), Ekman (T_{EK}), and upper mid-ocean (T_{UMO}) transports, *Kanzow et al.* [2010] found that T_{UMO} is the largest contributor to the seasonal cycle of the AMOC, with a peak-to-peak seasonal amplitude of 5.9 Sv. They found that the T_{UMO} has its highest (lowest) southward flow in April (November) and therefore the AMOC has its lowest (highest) northward transport in April (November). *Zhao and Johns* [2014] extended that analysis of the RAPID-MOCHA array data to the first 7 years and found a similar pattern.

Kanzow et al. [2010] explained 4.3 Sv of the seasonal cycle of the AMOC using a linear Rossby wave model that simulates the response of T_{UMO} to the seasonal cycle of the wind stress curl along 26.5°N. Their results imply that the baroclinic response of the interior component of the AMOC depends on the density

differences between the eastern and western boundaries, which are related, in first order, to the wind stress curl forcing at these boundaries. They concluded that the seasonal variation of T_{UMO} is almost entirely due to changes in stratification at the eastern boundary, which is caused by local wind stress curl variations. Based on the results of *Chidichimo et al*. [2010], that report no significant seasonal density anomalies deeper than 100 m in the RAPID-MOCHA moorings located 1000 km offshore of the African slope, *Kanzow et al*. [2010] state that the transport anomalies dominating the seasonal cycle of T_{UMO} do not correspond to basin-scale coherent flows but rather to flows concentrated within a narrow band along the eastern boundary. In contrast with these studies, *Yang* [2015], using model simulations, found that the seasonal variability of the AMOC at 26.5°N is due to the redistribution of water mass, driven by both, local and remote wind stress forcing. In this context, it is natural to ask if this strong seasonal cycle has been observed along the eastern region of the North Atlantic Subtropical Gyre, and specifically near the RAPID-MOCHA moorings at the African slope.

The eastern region of the North Atlantic Subtropical Gyre, around the Canary Islands, includes the southward flowing Canary Current (CC). The first studies of the CC, using historical hydrographic data [*Stramma*, 1984; *Stramma and Siedler*, 1988; *Stramma and Müller*, 1989], determined a seasonal change in the structure of the subtropical gyre, with the CC flowing closer to the African coast in summer. Some authors have found that the variability of the CC in the oceanic region of the Canary Islands, i.e., far away from the continental slope, is driven by the wind, and its transport is well explained by the Sverdrup balance [*Fraile-Nuez and Hernández-Guerra*, 2006; *Mason et al*., 2011]. Using one hydrographic cruise per season north of the Canary Islands, *Machín et al*. [2006] reported that the seasonal cycle for the oceanic region of the of the CC at 32°N ranges between the lowest transport of 2.8 ± 1.0 Sv southward in April (the authors suggested that the low value in winter is the result of a migration out of the sampled region of the CC), to the highest transport of 4.5 ± 1.2 Sv southward in fall. *Pérez-Hernández et al*. [2013] confirmed that CC in the oceanic region of the Canary Islands migrates offshore in fall and has a transport of 5.8 ± 0.2 Sv southward. *Hernández-Guerra et al*. [2003] found that the variability in the flow through the Lanzarote passage (LP) was different than the variability of the CC in the oceanic region of the Canary Islands, attributing this difference to different forcing, and therefore different dynamics driving the flow in the two areas. These authors found that during fall, the flow in the LP reverses its direction, with a mean northward transport of 1.7 ± 0.2 Sv for the North Atlantic Central Water (NACW) and the surface waters [*Hernández-Guerra et al*., 2003]. For the NACW and intermediate waters, *Machín et al*. [2010] attributed the northward flow during fall to isopycnal stretching due to wind forcing. In the NACW and SW, *Pérez-Hernández et al*. [2015] attributed the northward flow during fall in the LP to the recirculation of the CC. For the surface waters, some authors [*Pelegrí et al*., 2005; *Laiz et al*., 2012] have also associated this reversal in the LP with the upwelling off northwest Africa and the associated Canary Upwelling Current (CUC).

Due to the important role attributed to the eastern Atlantic, in this study, we describe the seasonal cycle of the eastern region of the North Atlantic Subtropical Gyre in the Canary Islands that includes the CC and the flow through the LP. We use hydrographic data from two cruises carried out in a box-shaped domain around the Canary Islands, in the region where the eastern component of the RAPID-MOCHA array is located (Figure 1). CTD, VMADCP, and LADCP data are combined with inverse modeling in order to determine absolute geostrophic transports in the Canary Islands region during fall and spring. The objective of this paper is to show whether there is a dramatic change in the circulation between April and October, and if the circulation of the CC and the flow through the LP have different dynamics, associated with different forcing mechanisms. We also include a sensitivity study of the linear Rossby wave model used by *Kanzow et al*. [2010] to determine if this model is appropriate to describe the seasonal cycle of the CC and the flow through the LP and, therefore, open the question about its appropriateness for explaining the seasonal cycle of the AMOC. We hypothesize that the seasonal cycle of the LP is due to the recirculation of the Canary Current and to the seasonal cycle of the poleward flow that characterizes the eastern boundaries of the oceans.

The remainder of the paper is organized as follows. In section 2, the different data sets are described. In section 3, we show the main results: the circulation around the Canary Islands estimated using the geostrophic approach and using an inverse model. We also assess the representativeness of the observations. In the next section, the discussion, we describe the sensitivity study of the linear Rossby wave model and discuss the appropriateness of this model to explain the seasonal cycle of the CC and the flow at the eastern boundary. We finish with the conclusions in section 5.
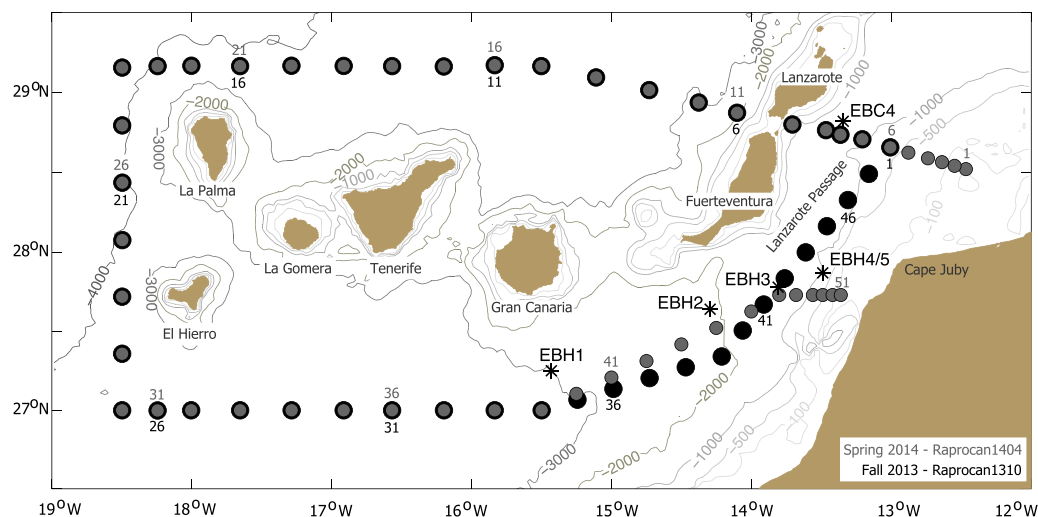
Figure 1. Map of the study area showing the main topographic and geographical features referred to in the text. The 200, 500, 1000, and 2000 m isobaths are indicated with grey lines. The grey circles are the stations sampled in the spring cruise (Raprocan1404), and the black circles are the hydrographic stations that were sampled in the fall cruise (Raprocan1310). One in every five stations for each cruise has been labeled. The asterisks indicate the position of the main moorings of the RAPID-MOCHA array at the eastern boundary, and the mooring EBC4.

2. Data

2.1. Hydrographic Data

Two hydrographic cruises were carried out in fall 2013 (48 stations, 15–25 October) and spring 2014 (51 stations, 4–14 April) as part of the Raprocan project, the Canary Islands component of the Spanish Institute of Oceanography ocean observing system [*Vélez-Belchí et al.*, 2015; *Tel et al.*, 2016]. During the fall cruise, the box-shaped domain was closed in the east by hydrographic stations, while during spring, the box was closed with the African coast (Figure 1). In each station, conductivity, temperature, and pressure were measured with redundant temperature and salinity sensors from a Seabird 911+ CTD. At each station, velocity data were acquired from a Lowered Acoustic Doppler Current Profilers (LADCP) system composed of a 150 kHz LADCP downward looking (master) and a 300 kHz LADCP upward looking (slave), with a shared battery pack. The LADCP data were processed according to *Fischer and Visbeck* [1993]. LADCP and Ship mounted Acoustic Doppler Current Profilers (SADCP) data were used to estimate the velocity in the assumed layer of no-motion by comparing the LADCP and SADCP velocity profiles with the geostrophic velocity profile at each station as indicated in *Comas-Rodríguez et al.* [2010]. Data were acquired at each station from the surface down to 10 m above the bottom. Distance intervals between stations were approximately 50 km except for the stations over the African slope, which were 4–5 km apart. Temperature and pressure sensors were calibrated at the SeaBird laboratory before the cruise. On board salinity calibration was carried out with a Guildline Autosal model 8400B salinometer with a precision better than 0.002 for single samples.

2.2. Mooring Data

A mooring, named EBC4, has been maintained, with gaps, since 2000 in the LP at 28°14″N 13°28″W, with a lower depth of 1280 m (Figure 1). The mooring contains five NORTEK current meters and five microSBE37, at 116, 291, 517, 873, and 1204 m, which record velocity, temperature, salinity, and pressure. The first three current meters are located in the upper layers, occupied by North Atlantic Central Waters (NACW); the next two current meters are in intermediate layers that contain Antarctic Intermediate Waters (AAIW) and Mediterranean Waters (MW), respectively. The sampling time interval for the instruments is 2 h. In this paper, we have used data collected between October 2013 and April 2014.

2.3. Sea Level Data

Maps of sea level anomaly (MSLA) were obtained from the Space Oceanographic Division of Collecte Localization Satellite through the Archiving, Validation and Interpretation of Satellite Oceanographic Data project.

The MSLA is a merged product from all available Sea level Anomaly data from TOPEX/Poseidon, Jason-1, Jason-2, Envisat, and GFO satellites. The MSLA data have a temporal resolution of 1 day and are gridded in $0.25° \times 0.25°$ spatial bins on a Mercator grid.

3. Results

3.1. Water Mass Distribution

In the Canary basin, the waters above the seasonal thermocline, $\gamma^n < 26.850$ kg m^{-3}, are characterized on the θ/S diagram by scattered temperature and salinity values due to seasonal heating and evaporation (Figure 2). These waters occupy the upper 300 m in the oceanic region, and the upper 100 m in the stations under the effect of the coastal upwelling, and are considered the surface waters (SW). During spring (Figure 2a), the stations on the eastern side of the Lanzarote passage (LP) and near Cape Juby have lower salinities and temperatures, due to the effect of the coastal upwelling that is stronger than during fall (Figure 2b).

Below the seasonal thermocline and through the permanent thermocline is the North Atlantic Central Water (NACW), roughly delimited by $26.850 < \gamma^n < 27.380$ kg m^{-3}, between 300 and 700 m depth [*Hernández-Guerra et al.*, 2005]. These waters are characterized on the θ/S diagram, both in spring and fall, by an approximately straight line relationship between potential temperature ($11.4°C < \theta < 14.9°C$) and salinity ($35.6 < S < 36.1$). NACW was sampled in all the stations during the spring and fall cruises, with the waters in the LP showing slightly lower temperature values.

At intermediate levels, between $27.380 < \gamma^n < 27.820$ kg m^{-3}, two distinct water masses are found in the Canary basin, the fresher ($S < 35.3$) and slightly lighter Antarctic Intermediate Waters (AAIW), and the saltier ($S > 35.4$) and heavier Mediterranean Waters (MW) [*Hernández-Guerra et al.*, 2001]. The MW, found in both seasons and mostly in the northern hydrographic section, has the highest salinity (>36) on the southern hydrographic section during spring 2014. This high salinity is due to a MEDDY (Mediterranean Water eddy), centered at approximately 1000 m and 18.5°W, which carries the purest MW (warmer and saltier) within its core. The AAIW is also found in both seasons, mostly in the southern hydrographic section and in the vicinity of the African slope (LP and Cape Juby). During both seasons the purer AAIW is found in the southern hydrographic section. The purest AAIW is found during fall, with salinities as low as 35.157. During fall the AAIW is more abundant closer to the African coast, while during the spring the AAIW spreads out toward the west.

3.2. Geostrophic Transport

To describe the seasonal change in the ocean circulation in the Canary basin, we initially estimated the mass transports using geostrophic velocities referenced at a level of no-motion at $\gamma^n = 27.975$ kg m^{-3} (roughly 1950 m), below the interface between the MW and the NADW, for the oceanic region; and $\gamma^n = 27.380$ kg m^{-3} (roughly 750 m) in the interface between the AAIW and the MW for the stations in shallower waters. These reference levels have been used previously in the area [*Hernández-Guerra et al.*, 2005]. The mass transport was estimated along 13 neutral density layers. The surface waters (SW) occupy the first two layers, NACW occupies the next two layers, the intermediate water masses the next three, and the deep water masses are found in the densest layers (see Table 1). In the remainder of the paper, we will focus on the transport relevant to the upper ocean branch of the AMOC, this is the one associated with the SW, NACW and the intermediate water masses.

Far away from the continental slope, in the oceanic region, the CC is driven by the wind, and its transport follows the Sverdrup balance [*Fraile-Nuez and Hernández-Guerra*, 2006; *Mason et al.*, 2011], while the coastal upwelling and the poleward flow characteristics of eastern ocean boundaries, under the influence of the continental slope, drive the ocean on both sides of Lanzarote. Based on that, we carry out the analyses separately for both regions, the oceanic region, and the region under the influence of the continental slope and the coastal upwelling. We use the term eastern boundary (EB) to include both sides of Lanzarote, i.e., the LP and the area just west of Lanzarote, both under the influence of the continental slope circulation.

To point out the differences between the oceanic region and the waters at the EB, we have integrated the mass transport separately in the oceanic stations and in the EB for spring and fall, choosing the stations for each region based on the water masses analysis and the circulation patterns (Figure 3). As, we will describe later, we attribute this differences to different forcing mechanisms and therefore to different dynamics for
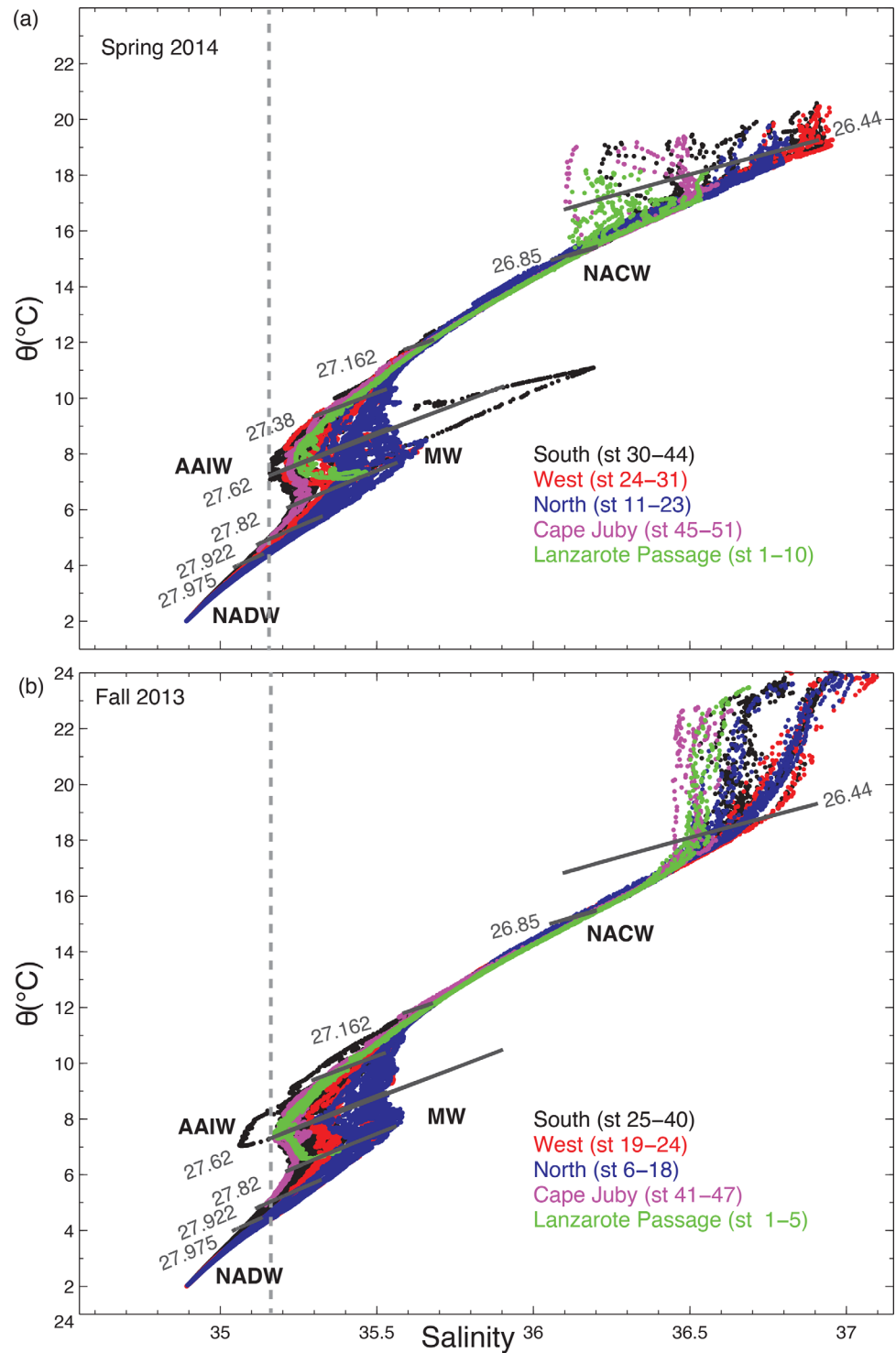
Figure 2. θ/S diagram for the (a) spring (Raprocan1404) and (b) fall (Raprocan1310) cruises. The grey thick lines correspond to the isoneutrals used in the inverse model (see Table 1). The colors of the dots, as indicated in the legend, correspond to the three sections (northern, southern, and western) and the stations in the LP for each cruise. The vertical dashed grey line corresponds to the minimum salinity value found in the intermediate waters during spring (S = 35.157). NACW stands for North Atlantic Central Water, MW for Mediterranean Waters, AAIW for Antarctic Intermediate Waters, and NADW for North Atlantic Deep Waters.

each area. During both seasons, the transports of the SW and the NACW ($\gamma^n < 27.380$ kg m^{-3}) in the oceanic region is southward, flowing through the Canary Island archipelago (Figures 3b and 3d). The transport through the northern section is approximately the same as that through the southern and western sections.
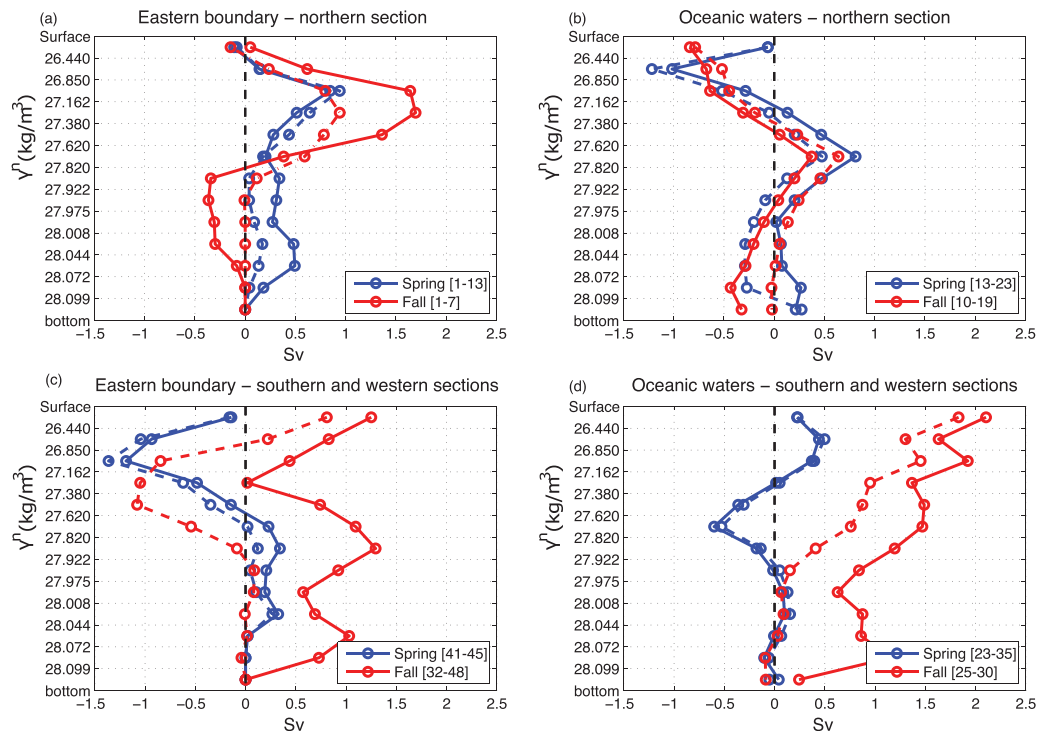
Figure 3. Integrated mass transport (1 Sv = 1×10^9 kg/s^{-1}) per layer for the spring and fall cruises using the geostrophic velocities (dashed) and the geostrophic velocities corrected with the LADCP velocities (solid). The four panels correspond to the transport through (a) the northern and (c) western-southern sections at the eastern boundary, that includes the Lanzarote passage and the flow just west of Lanzarote; and (b) the northern and (d) western-southern sections of the oceanic region. The hydrographic stations used to compute the integrated mass transport per layer for the oceanic region and the eastern boundary are indicated in the legend. Positive sign is for divergent flow, i.e., out of the box; while negative sign is for convergent flow, i.e., into of the box. In the northern section, southward flow will be negative; in the westward section, eastward flow will be negative; and in the southern section, southward flow will be positive.

The transport in the oceanic region in spring and fall presents a similar vertical behavior, with approximately the same transport flowing southward in the northern and southern (including the western) sections, independently of the transport in the EB.

We have estimated, within the volume delimited by the box-shaped domain of hydrographic stations for the spring cruise, and the hydrographic stations and the African coast for the fall survey, the total accumulated geostrophic net mass transport. During spring (fall), this geostrophic net mass transport shows an imbalance of −1.30 Sv (−0.50 Sv) for the SW, −1.60 Sv (−1.70 Sv) for the NACW, and −1.0 Sv (−0.90 Sv) for the intermediate waters (Figure 4).

To determine more precisely the transport at the different layers, we corrected the initial geostrophic velocities using the LADCP velocities averaged where the geostrophic shear and the LADCP velocities were closest for each station [*Comas-Rodríguez et al.*, 2010]. However, the use of the LADCP velocities does not totally correct the imbalance (Figure 4), neither for spring nor fall. Mostly, the LADCP velocities correct the geostrophic velocities in the southern and northern sections of the LP. The level of no-motion used in the shallower waters (γ^n = 27.380 kg m^{-3}) of the LP corresponds to the interface between the MW and the AAIW, and this interface changes rapidly due to the strong interaction between the
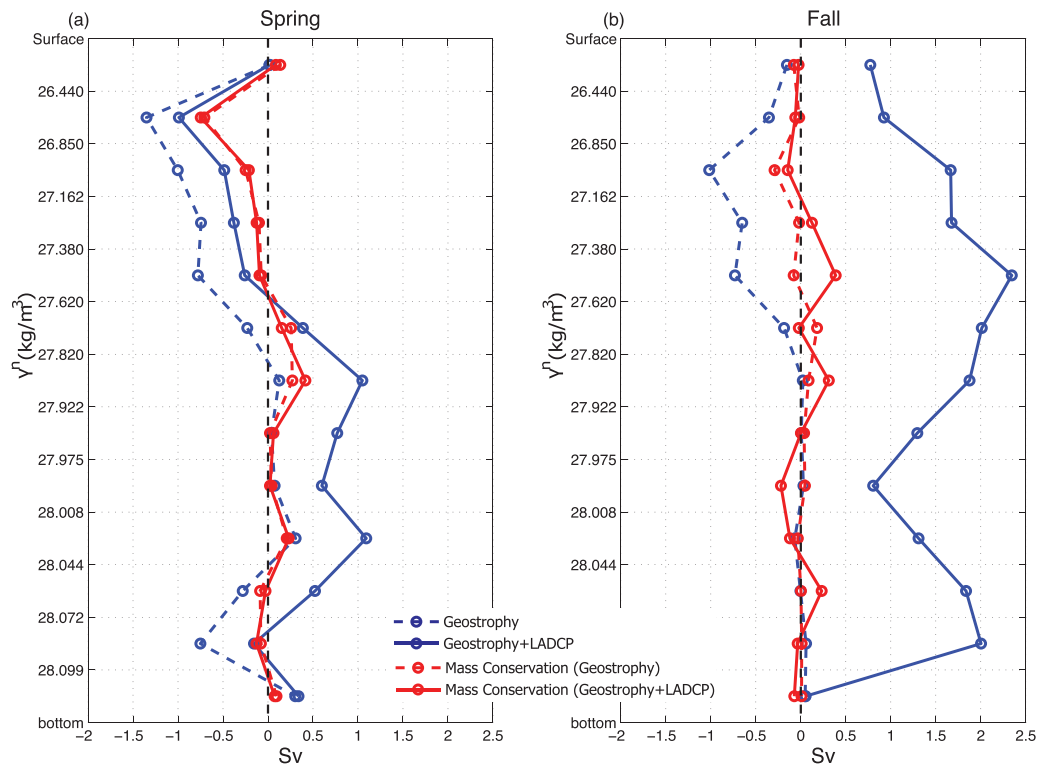
Table 1. Deepest Limit (dbar) of the γ^n Isoneutral Layers Used in the Mass Transport Analyses

Layer	γ^n (kg m^{-3})	Deepest Limit (dbar)	Water Masses
1	26.440	20	SW
2	26.850	298	SW
3	27.162	540	NACW
4	27.380	740	NACW
5	27.620	967	AAIW
6	27.820	1314	AAIW, MW
7	27.922	1656	NADW
8	27.975	2015	NADW
9	28.008	2241	NADW
10	28.044	2592	NADW
11	28.072	2965	NADW
12	28.0986	3519	NADW
13	28.1295 (bottom)	3923	NADW

Figure 4. Total integrated mass transport (Sv) along the box-shaped domain per layer for (a) the spring and (b) the fall cruises using the geostrophic velocities (blue, dashed), the geostrophic velocities corrected with the LADCP velocities (blue), inverse model velocities obtained using the geostrophic velocities as initial guesses (red, dashed), and inverse model velocities obtained using the geostrophic velocities corrected with the LADCP velocities as initial guesses (red). Positive sign is for divergent flow, i.e., out of the box; while negative sign is for convergent flow, i.e., into of the box.

opposing flows of the intermediate water masses. Moreover, this interface will change with the season, since, as we will describe later, there is a strong change in the circulation in the LP between spring and fall. In order to obtain a better estimate of the velocities at the reference level, we use an inverse model.

3.3. Inverse Model

To reduce the mass transport imbalance obtained using the geostrophic and LADCP velocities, and therefore increase the reliability of the mass transport estimates, we use an inverse box model that based on the conservation of mass allow us to estimate the velocities at the reference level. Following *Hernández-Guerra et al.* [2005] and *Pérez-Hernández et al.* [2013], we applied an inverse model to the volume delimited by the box-shaped domain of hydrographic stations, and the African coast in the case of the fall survey. The box model includes the conservation of mass per layer, the total, and an adjustment for the initial Ekman transport:

$$\iint \rho b \ dx \ dz = - \iint \rho V_{rel} \ dx \ dz + E_k \qquad (1)$$

where x and z are the along box transect and vertical coordinates, respectively; ρ is the density at each interface. The integral terms are derived from the reference velocity (b) and the relative velocity (V_{rel}). The term E_k designates the Ekman transport.

Once discretized, the equations of mass per layer and the total form the following matrix equation:

$$A \ x + n = -\Gamma \qquad (2)$$

where A is a matrix with size the number of layers (Q)×stations (N), n is a column vector whose elements are the noise for each equation, Γ is a vector representing the degree of initial imbalance in each layer, and x is the column vector containing the unknowns of the system:
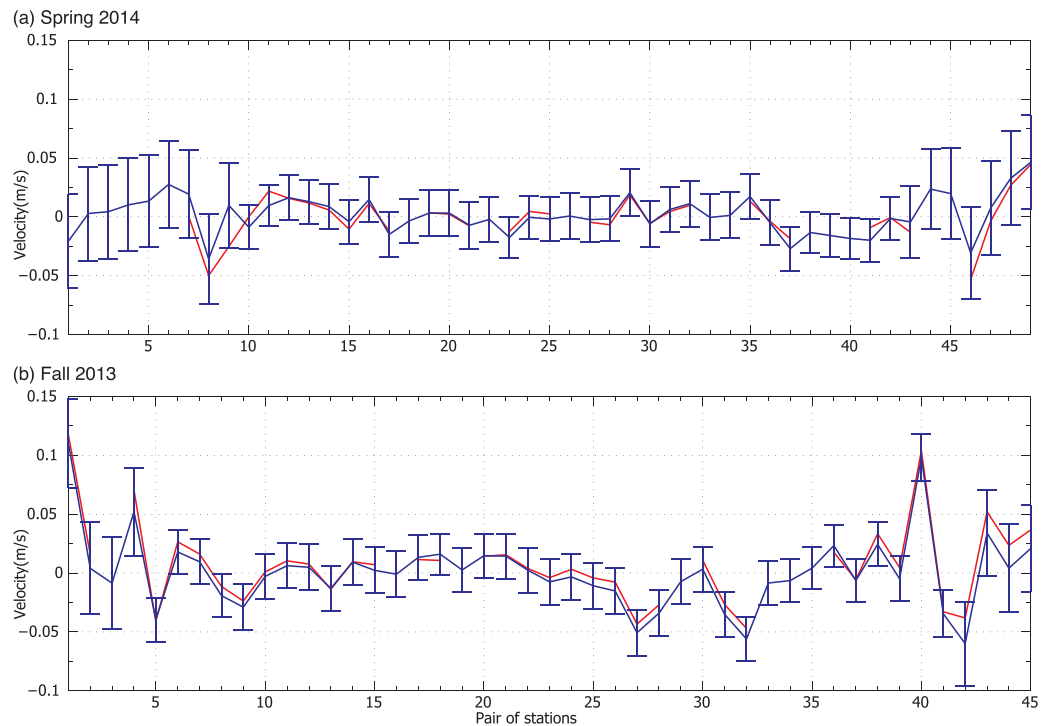
Figure 5. Velocities at the reference level obtained using the LADCP data (red line) and the inverse model (blue line) for (a) the spring (Raprocan1404) and (b) the fall (Raprocan1310) cruises. Positive sign is for divergent flow, i.e., out of the box; while negative sign is for convergent flow, i.e., into the box.

$$\begin{pmatrix} (b_i), & i=1,\dots N_{pair} \\ & \Delta T_{Ek} \end{pmatrix} \tag{3}$$

To solve the inverse problem, we applied the Gauss-Markov method which produces a minimum error variance solution from the initial estimates of the unknowns. Since the solution provided by the method depends on the variance of the velocity field, we have used a priori variance of mass transport of $(1.5\ \mathrm{Sv})^2$ for the surface layer, $(1\ \mathrm{Sv})^2$ for the intermediate layers, $(0.5\ \mathrm{Sv})^2$ for the deep layers and $(4\ \mathrm{Sv})^2$ for the total [*Pérez-Hernández et al.*, 2013].

The main outcomes of the inverse modeling are the velocities at the reference level, along with their error covariance. The difference between these velocities and the initial geostrophic velocities referenced to the LADCP measurements is small, in the range 1–2 cm s^{-1} for both seasons (Figure 5). The largest differences are in the shallower stations, in the LP and west of Lanzarote. In these stations, the level of no-motion used ($\gamma^n = 27.380\ \mathrm{kg\ m}^{-3}$) corresponds to the interface between the MW and the AAIW. This interface changes dramatically due to the strong interaction between the opposite flowing intermediate water masses and, therefore, is different for each cruise. The uncertainties are quite similar to the imposed a priori variances, in agreement with other inverse model results [*Hernández-Guerra et al.*, 2014; *Hernández-Guerra and Talley*, 2016].

3.4. Adjusted Geostrophic Transport
The velocities at the reference level estimated using the inverse model allow us to compute the adjusted geostrophic mass transport (Figure 6). Using the inverse modeling results, the total adjusted geostrophic mass transport imbalance during spring (fall) is -0.7 ± 0.2 Sv (-0.1 ± 0.2 Sv) for the SW, -0.3 ± 0.3 Sv (-0.0 ± 0.3 Sv) for the NACW, and -0.1 ± 0.3 Sv (-0.4 ± 0.4 Sv) for the intermediate waters.

As observed with the geostrophic transport, during both seasons the transports of the SW and the NACW in the oceanic region is southward, flowing through the Canary Island archipelago. In the oceanic region (Figures 6b and 6d), and for the SW, NACW, and intermediate waters ($\gamma^n < 27.820\ \mathrm{kg\ m}^{-3}$), the transport through the northern section is approximately the same that the transport through the western and
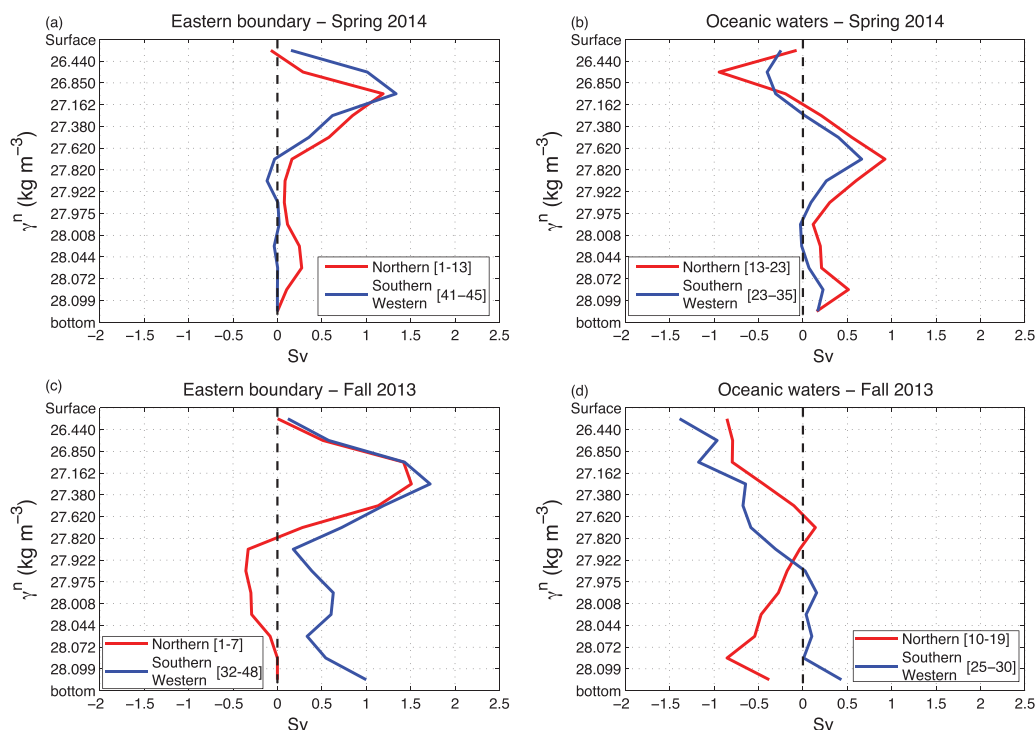
Figure 6. Total integrated mass transport (Sv) per layer computed using the absolute geostrophic velocities estimated by the inverse model with the geostrophic velocities corrected with the LADCP velocities as the initial guess. The transport has been integrated in two regions, (a, c) the eastern boundary and (b, d) the oceanic region; for the spring (Figures 6a and 6b) and fall cruises (Figures 6c and 6d). For the two regions, the red (blue) line denotes the transport through the northern (southern and western) hydrographic sections. The hydrographic stations used to compute the transport for each region are indicated in the legend. Positive sign is for divergent flow, i.e., out of the box; while negative sign is for convergent flow, i.e., into of the box. In the northern section, southward flow will be negative; in the westward section, eastward flow will be negative; and in the southern section, southward flow will be positive.

southern sections, with a very similar vertical distribution. In the EB (Figures 6a and 6c), and for the SW, NACW, and intermediate waters ($\gamma^n < 27.820$ kg m^{-3}), the transport in the EB shows also a very similar vertical structure for spring and fall, and the transport through the northern section exits through the western and southern sections. In the following sections, we describe in detail the circulation for spring and fall.

3.4.1. Spring 2014

During spring 2014, the mass transports in the EB and in the oceanic region of the Canary Islands are different (Figures 6a and 6b), and therefore we will describe the circulation during spring 2014 separately for both regions. Between stations 1 and 10 in the LP, the SW transport is 0.5 ± 0.2 Sv southward, while the transport of the NACW waters is not statistically significantly different from zero (0.4 ± 0.4 Sv). Just west of Lanzarote, between stations 11 and 12, there is a northward transport of 0.8 ± 0.2 Sv for the SW and 1.6 ± 0.30 Sv for the NACW waters. Between stations 13 (west of Lanzarote) and 23 (north of La Palma), there is a southward transport of 1.0 ± 0.4 Sv of SW, and a not statistically significantly different from zero transport of NACW. This southward flow is the CC. There is an eastward geostrophic mass transport of 0.9 ± 0.3 Sv for the SW and 1.2 ± 0.4 Sv for the NACW waters that enter the box-shaped domain through its western section (stations 23–30). Part of these eastward SW and NACW mass transport recirculates anticyclonically southwest of El Hierro, and the rest joins the southward flowing CC. Most of the CC southward transport observed in the northern and western section flows through the archipelago and exits the box-shaped domain through its southern section (stations 30–35).

The accumulated transport through the southern section, south of Gran Canaria and Fuerteventura, is disturbed by a cyclonic eddy formed downstream of the Canary Island archipelago, and by an anticyclonic eddy south of Fuerteventura, previously detected by satellite images [*Hernández-Guerra et al.*, 1993; *Pacheco and Hernández-Guerra*, 1999]. The strength of the cyclonic eddy south of Gran Canaria is 4.1 ± 0.4 Sv for the SW and 4.0 ± 0.4 Sv for the NACW waters, while the anticyclonic eddy south of Fuerteventura has a strength nonstatistically different from zero for the SW, and of 0.7 ± 0.4 Sv for the NACW waters. Since these eddies
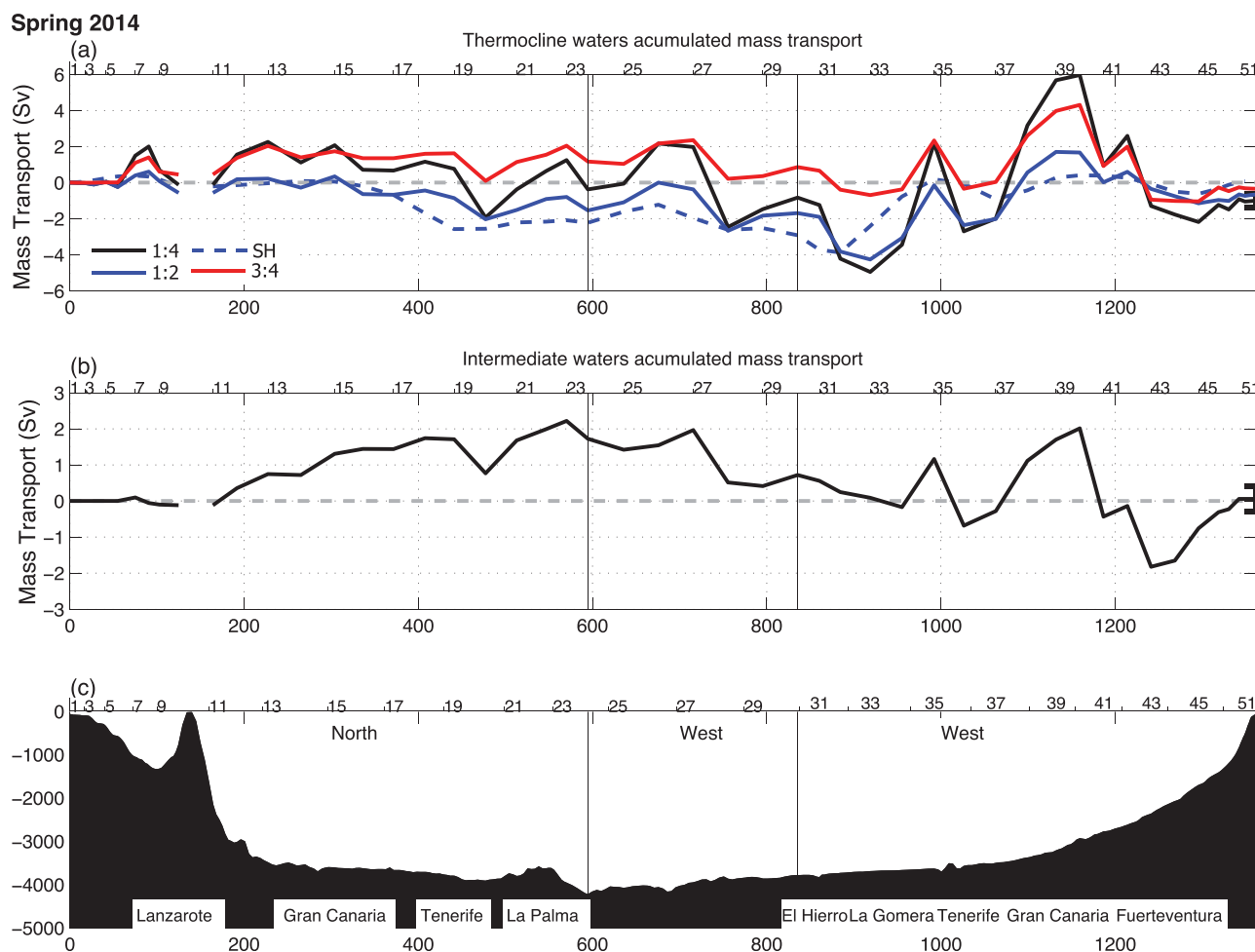
Spring 2014

Figure 7. (a) Accumulated mass transport (Sv) during the spring cruise (Raprocan1404) for the surface (blue), NACW (red), and total upper ocean waters (black). The dashed blue line is the accumulated mass transport obtained using the geostrophic velocities at the surface from the altimetric mean dynamic topography (SH) and integrating them to the depth corresponding to the lower limit of the seasonal thermocline waters. The accumulation of the mass transport has been computed following the stations, and therefore the x axis corresponds to the distance from the first station. For reference the stations are labeled on the top axis. (b) Accumulated mass transport during the spring cruise for the intermediate waters (layers 5 and 6). (c) Depth of the bottom. For reference, each of the sections, northern, western and southern; and the position of the Canary Islands are indicated. Positive sign is for divergent flow, i.e., out of the box; while negative sign is for convergent flow, i.e., into the box. In the northern section, southward flow will be negative; in the westward section, eastward flow will be negative; and in the southern section, southward flow will be positive.

are well sampled, the associated transport through the southern section is not statistically significantly different from zero. Taking into account the transport of these eddies, we estimate that south of Fuerteventura there is a northward transport of 1.2 ± 0.2 Sv for the SW and 1.3 ± 0.3 Sv for the NACW waters. This northward transport is coherent with the northward transport at both sides of Lanzarote observed in the northern section.

For the intermediate waters in spring 2014 (Figure 7b), the mass transports in the EB and in the oceanic region of the Canary Islands are also different. In the LP, the transport is southward, although not statistically significantly different from zero (0.1 ± 0.4 Sv); in the southern section of the LP it is 0.6 ± 0.4 Sv southward. In the oceanic region, the transport is northward. Between stations 11 and 23, there is a 1.8 ± 0.3 Sv northward transport of intermediate waters. These waters enter the box through the western section, between stations 25 and 31 (1.0 ± 0.6 Sv) and through the southern section, between stations 31 and 36 (0.9 ± 0.5 Sv). The accumulated transport through the southern section, south of Gran Canaria and Fuerteventura, is also disturbed by a cyclonic eddy formed downstream of the Canary Island archipelago, although weaker than the signal at shallower layers; and by an anticyclonic eddy south of Fuerteventura. The strength, at the intermediate layers, of the cyclonic eddy south of Gran Canarias is 2.2 ± 0.4 Sv, while the anticyclonic eddy south of Fuerteventura has a strength of 1.3 ± 0.3 Sv. This anticyclonic eddy is stronger
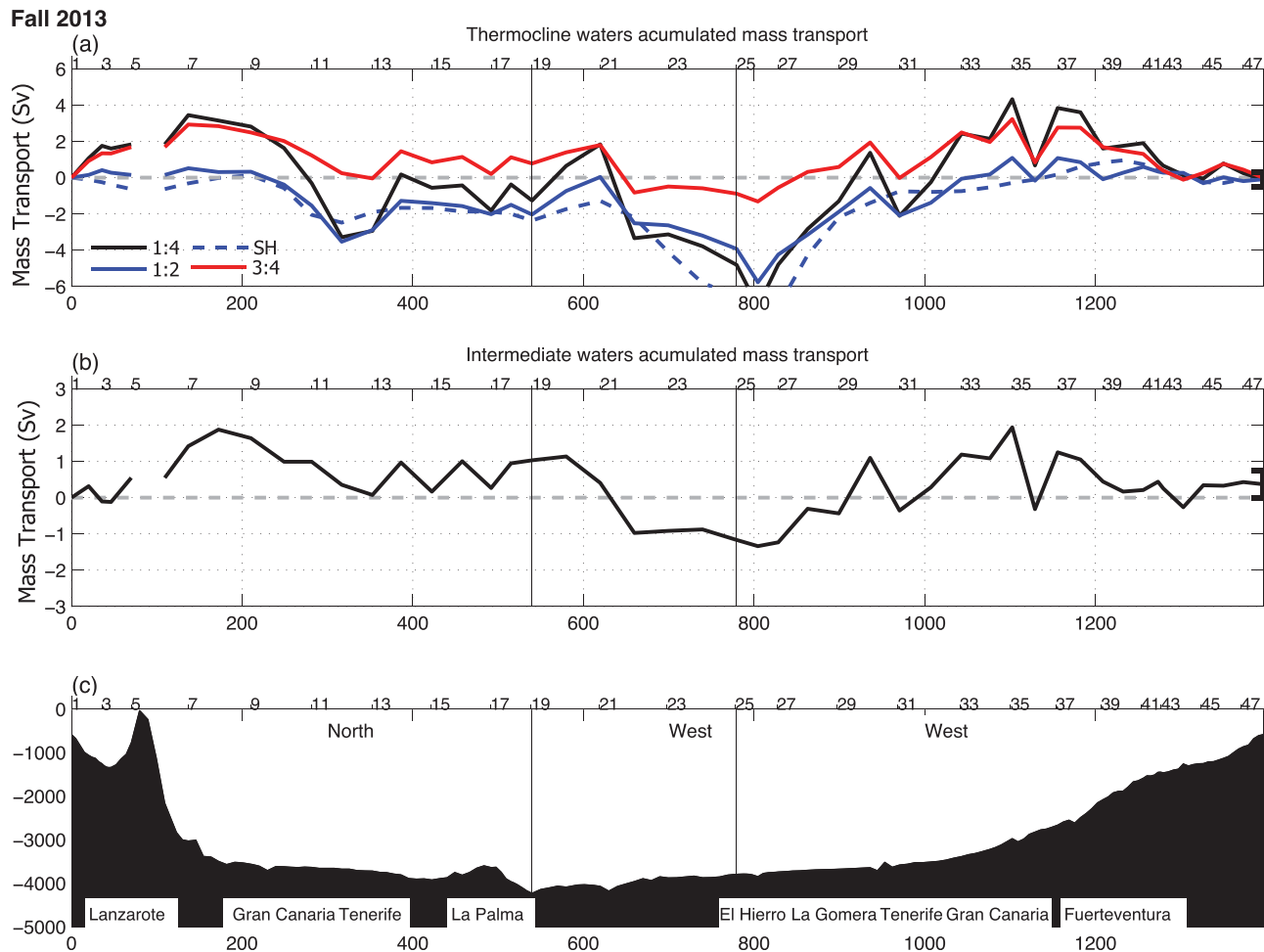
Fall 2013

Figure 8. As Figure 7, but for the fall cruise (Raprocan1310).

that the anticyclonic circulation found in the surface and NACW waters, suggesting that this eddy lying close to the African slope is associated with the interaction of the intermediate waters with the bottom topography, since this eddy was close to the 1000 m isobath.

3.4.2. Fall 2013

In the EB during fall 2013 (Figure 8), there is a 1.7 ± 0.4 Sv northward transport of NACW in the LP, and a 1.6 ± 0.2 Sv northward transport of NACW west of Lanzarote, between stations 6 and 7 (Figure 8a). In the oceanic region, between stations 7 and 19, the CC carries southward a total of 2.9 ± 0.6 Sv between the SW (1.6 ± 0.6 Sv) and the NACW (1.2 ± 0.5 Sv). A second branch of the CC transports 2.1 ± 0.5 Sv of SW (0.5 ± 0.2 Sv) and NACW (1.6 ± 0.5 Sv) into the box through the western section (Figure 8a). The CC flows out of the box between stations 28 and 32, with a total southward transport of 4.2 ± 0.4 Sv (2.6 ± 0.2 Sv for SW and 1.6 ± 0.3 Sv for NACW). This transport is coherent, within the uncertainty, with the transport of the CC in the northern and western sections. Although an anticyclonic eddy with strength of 1.5 ± 0.4 Sv is observed southwest of El Hierro. Close to the coast of Africa between stations 38 and 43, there is a NACW northward transport of 3.3 ± 0.4 Sv, coherent with the northward transport found at both sides of Lanzarote in the northern section. South of Gran Canaria, there is a cyclonic eddy with a strength of 2.1 ± 0.4 Sv for the surface and NACW waters.

The transport of intermediate waters, as shown in the accumulated adjusted geostrophic mass transport (Figure 8b) is different in the oceanic region than at the EB. In the EB region, 0.5 ± 0.4 Sv flows northward through the northern section of the LP, and west of Lanzarote between stations 6 and 8 1.3 ± 0.4 Sv flows northward. These northward transports are coherent with the northward transport of 1.8 ± 0.5 Sv found between stations 35 and 42 in the southern section. In the oceanic region of the northern section, there is a
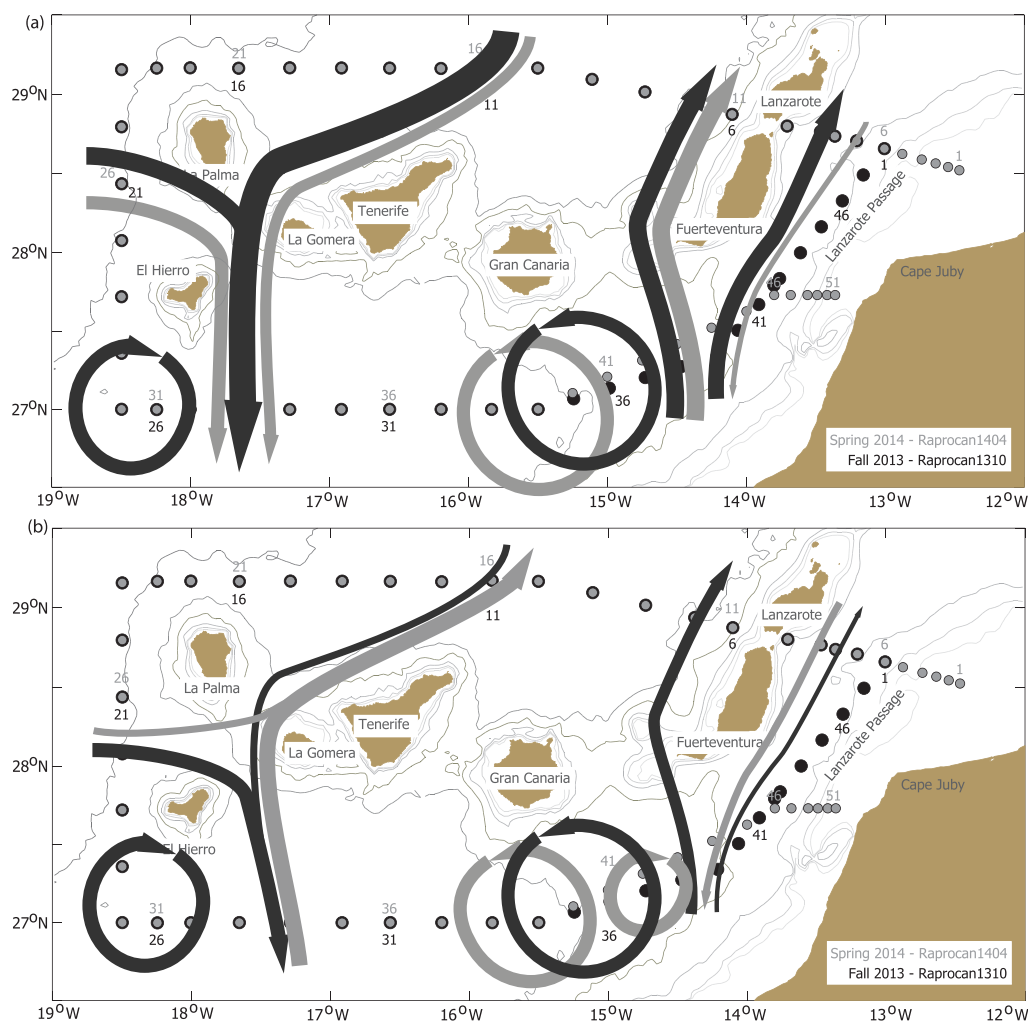
Figure 9. Schematic diagram of the mass transport during the fall and spring cruises for (a) the SW and NACW and (b) the intermediate waters. For reference, the main topographic and geographical features referred to in the text are indicated.

southward transport of 0.8 ± 0.7 Sv between stations 8 and 19. This flow joins the 1.9 ± 0.5 Sv of eastward transport that entered the box though the western section, and 2.3 ± 0.60 Sv flows out of the box southward between stations 25 and 31 in the southern section. South of Gran Canaria and Fuerteventura, delimited by the 1000 m isobath, there is a cyclonic eddy (also observed in the NACW waters) with strength of approximately 1.8 ± 0.2 Sv. This observed reversal of the flow for the lower NACW and AAIW is coherent with the water mass distribution, with the purest AAIW flowing close to the African slope during fall.

3.5. Amplitude of the Seasonal Cycle

A diagram summarizing the mean circulation pattern for the SW, the NACW, and the intermediate waters is drawn in Figure 9, and a summary of the transport in the southern section can be found in Table 2. The analysis of the data from the hydrographic cruises and the inverse modeling indicates that there is a significant difference in transport between spring and fall, both in the oceanic region and in the EB. Since we have demonstrated that the flow in the southern section was coherent with the observations in the northern section, and that the total CC flowed through the southern section, including the contribution from a second branch that flowed through the western section, we focus the discussion on the seasonal cycle found at the southern section, the closest to the eastern component of the RAPID-MOCHA array [*Cunningham et al.*, 2007].

During spring in the oceanic region of the southern section, the CC transported a total of 2.4 ± 1.1 Sv southward, divided into layers as follows: 1.3 ± 0.4 Sv of SW, 0.2 ± 0.5 Sv of NACW, and 0.9 ± 0.5 Sv of

Table 2. Mass Transport (1 Sv = 1 × 10^9 kg/s^{-1}) Through the Southern Section for the CC and the Flow in the EB, That Includes the Flow Just West of Lanzarote and in the Lanzarote Passage for Spring and Fall[a]

		CC	EB	West of Lanzarote	Lanzarote Passage
Spring	SW	−1.3 ± 0.4	+0.7 ± 0.2	+1.2 ± 0.2	−0.5 ± 0.2
	NACW	−0.2 ± 0.5	+1.3 ± 0.3	+1.3 ± 0.3	0
	IW	−0.9 ± 0.5	−0.6 ± 0.4		−0.6 ± 0.4
	Net transport	*−2.4 ± 1.1*	*+1.4 ± 0.5*	*2.5 ± 0.4*	*−1.1 ± 0.4*
Fall	SW	−2.6 ± 0.2	+0.4 ± 0.1	+0.4 ± 0.1	0
	NACW	−1.6 ± 0.3	+2.9 ± 0.4	+1.2 ± 0.3	+1.7 ± 0.4
	IW	−2.3 ± 0.0	+1.8 ± 0.4	+1.3 ± 0.4	+0.5 ± 0.4
	Net transport	*−6.5 ± 0.4*	*+5.1 ± 0.6*	*+2.9 ± 0.5*	*+2.2 ± 0.6*
Seasonal cycle	SW	−1.3 ± 0.4	−0.3 ± 0.1		
	NACW	−1.4 ± 0.5	+1.6 ± 0.4		
	IW	−1.4 ± 0.5	+2.4 ± 0.4		
	Total	−4.1 ± 0.5	+3.7 ± 0.4		

[a]The table also includes the amplitude (fall-spring) of the seasonal cycle of the transport estimated at the southern sections for both surveys. SW is for the surface waters, NACW for the North Atlantic Central Water layer, IW is for the intermediate water layer and Net transport is the sum of SW, NACW and IW. Positive (negative) is for northward (southward) transport.

intermediate waters (Table 2). Close to Africa, east of 15°W, there is a northward flow of 1.2 ± 0.2 Sv of SW and 1.3 ± 0.3 Sv of NACW that flows out of the box west of Lanzarote, in the northern section. Closer to the African coast, there is a southward flow of 0.5 ± 0.2 Sv of NACW that entered the box through the northern section (Figure 9 and Table 2). In the LP, there is a 0.6 ± 0.4 Sv southward transport of intermediate waters. Altogether during spring there is a northward transport of 0.7 ± 0.2 Sv SW, 1.3 ± 0.3 Sv of NACW, and a southward transport of 0.6 ± 0.4 Sv of intermediate waters.

During fall, in the oceanic region of the southern section, the CC transports southward 2.6 ± 0.2 Sv of SW, 1.6 ± 0.3 Sv of NACW, and 2.3 ± 0.60 Sv of intermediate (Figure 9 and Table 2). Close to Africa, east of 15°W, there is a total northward flow of 5.1 ± 0.6 Sv that flows out of the box west of Lanzarote, and through northern section of the LP. This flow carries 0.4 ± 0.1 Sv of SW, 2.9 ± 0.4 Sv of NACW, and 1.8 ± 0.4 Sv of intermediate waters.

Between fall and spring, the CC changes in magnitude. If we define the seasonal cycle as Transport$_{Fall}$-Transport$_{Spring}$, the seasonal cycle for the CC is −4.1 ± 0.5 Sv (Table 2). In contrast, the circulation in the LP changes seasonally in intensity and direction. In spring, the total transport in the LP is 1.1 ± 0.4 Sv southward, in the same direction that in the oceanic region but, in fall, the transport increases (2.2 ± 0.6 Sv northward) and the direction is opposed to the CC for the SW, the NACW, and the intermediate waters. Taking into account this overall common behavior for the circulation on both sides of Lanzarote, we group them together and estimate that the seasonal cycle in the EB, defined as before, is +3.7 ± 0.4 Sv (Table 2).

3.6. Representativeness of the Seasonal Cycle

Although the months when the cruises were carried out were chosen based on previous studies, and the results are compatible with those obtained by *Machín et al.* [2006] and *Pérez-Hernández et al.* [2013], it is necessary to demonstrate that the results are representative of the seasonal cycle in the oceanic region and at the EB. To demonstrate this representativeness, and given the small-scale variability observed in the mass transport and the uncertainty associated with the lack of synopticity, we will use two additionally data sets.

To address the representativeness of the hydrographic data, we deployed a mooring in the LP between fall 2013 and spring 2014. The mooring was deployed in the deepest part of the northern sector of the Lanzarote passage (Figure 1) and was designed to monitor the main water masses that flow through the passage. This mooring has already been demonstrated to be representative of the transport in the Lanzarote passage [*Hernández-Guerra et al.*, 2003]. In agreement with the observations from the hydrographic data, the mooring data show, for the NACW and the intermediate waters, that the flow is northward during part of fall, this is the last days in October and the first two weeks in November (Figures 10b and 10c) and gradually transitions to a southward flow. During spring, the flow is southward, with the maximum intensity around March. At the intermediate waters level (925 dbar, Figure 10d), the mooring observations agree with the hydrographic ones, with northward flow in October and southward flow just before the spring cruise. This seasonal pattern is coherent with the analyses of *Fraile-Nuez et al.* [2010] that used 9 years of data from EBC4,
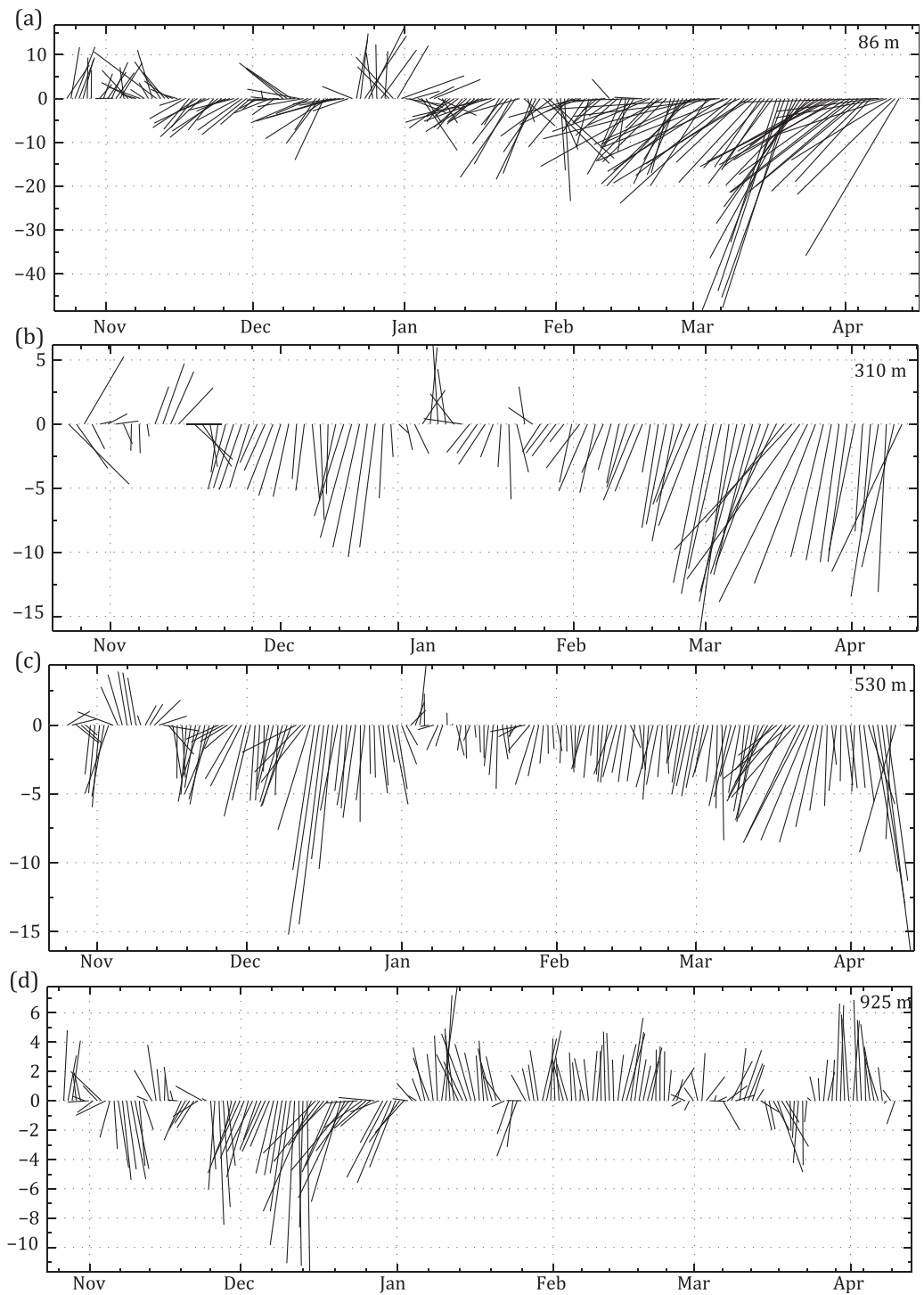
Figure 10. Low pass (>30 h) filtered velocities from October 2013 to May 2014, measured by four current meters installed in the EBC4 mooring at the (a) surface, (b, c) NACW, and (d) IW levels. Positive (negative) is northward (southward).

between 1997 and 2006 to show that for the NACW, the maximum southward transport was in winter and spring and the minimum was in summer and fall.

The reversal in the flow of the SW and NACW in the LP is also confirmed with sea level observations from altimetry (Figure 11). We computed the accumulated geostrophic transport along the ship track for both cruises as done with the hydrographic data, but using the altimetry data, and the depth of the
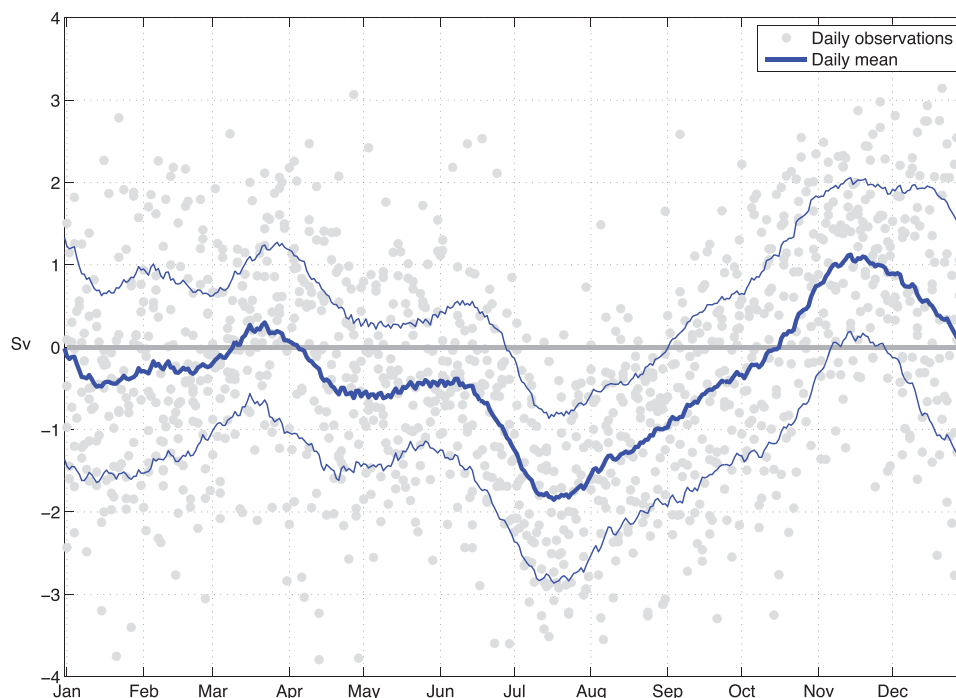
Figure 11. Mass transport estimates in the LP (Sv) using geostrophic velocities at the surface from the altimetric mean dynamic topography, and integrated down to the depth corresponding to the SW. The grey dots denote are the daily estimates in October 1992 to October 2014, the thick blue line is the daily mean and thick blue line is the mean plus one standard deviation. Positive (negative) is northward (southward).

$\gamma^n = 27.10$ kg m^{-3} ($\approx$500 dbar) as representative for the SW and the upper NACW. This altimetry estimation of the accumulated transport is very similar to the accumulated transport of the SW and the NACW obtained using the hydrographic data, as can be observed in Figures 7 and 8, where the altimetry estimations are shown. These estimations are highly correlated in spring (0.75) and fall (0.94) with the accumulated transport for the SW. During fall, the correlation is also high (0.74) for the NACW. For the LP (Figure 11) and in spite the high interannual variability, the altimetry data shows a strong mean seasonal cycle for the SW and upper NACW, with southward flow from January to October, and northward flow in fall, from October to the end of December. The maximum southward flow is during summer, in July, while the maximum northward transport is in November. The maximum southward transport in July is probably due to the upwelling jet associated with the northwest African upwelling system.

Once we have established that the altimetry data are an appropriate proxy for the circulation of the SW and for the NACW, it can be used to show whether the seasonal changes observed from the hydrographic cruises is representative. Using the approach described in the previous paragraph, that is also used by other authors [*Vélez-Belchí et al.*, 2013], we obtained a composite of the absolute sea level and the associated geostrophic velocities during spring and fall (Figure 12). During spring, the southward circulation in the oceanic region, west of Lanzarote, is weaker than in fall, coherent with the hydrographic observations, and the flow in the LP is weakly southward. During fall, the composite shows a strong recirculation cell at the easternmost islands of the Canary Island archipelago. In this cell, the main component is the southward flow west of Gran Canaria. The figure also shows the recirculation branch described by *Mason et al.* [2011] and *Pérez-Hernández et al.* [2013], that flows northward through the LP. The origin of the recirculation cell seems to be related to the pool of cold waters left by the gigantic filament south of Cape Ghir that develops in the summer, when the trade winds are stronger, as indicated by the minimum in the sea level observed in the composite at approximately 10°30″W, 31°30″N, a hypothesis also suggested by previous authors [*Pelegrí et al.*, 2005; *Mason et al.*, 2011]. Just south of Cape Bojador, the fall composite shows a strong anticyclonic eddy that is marginally observed with the hydrographic data set and that has been previously reported [*Ruiz et al.*, 2014].
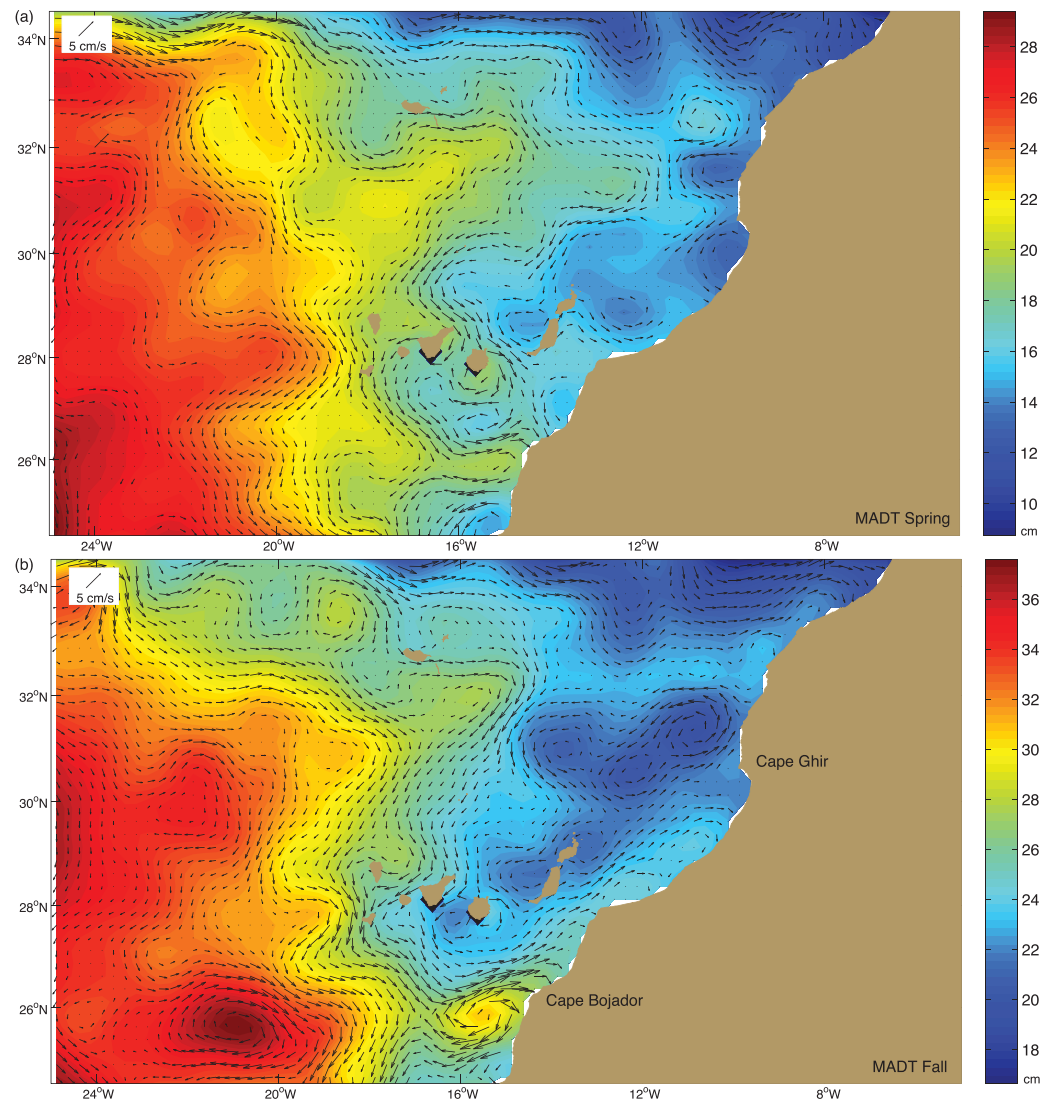
Figure 12. Composite of (a) spring and (b) fall MADT (Maps of Absolute Dhynamic Topography) and geostrophic velocity.

4. Discussion

We have shown that there is a dramatic change in the circulation between April and October. The seasonal cycle, defined as Transport_{Fall}-$\text{Transport}_{Spring}$, for the CC is -4.1 ± 0.5 Sv for the surface, central, and the intermediate waters. In the region east of 15°W, that we denominate EB, the seasonal cycle is $+3.7 \pm 0.4$Sv. We have also shown that the circulation of the CC and in the EB have different variability. The circulation in the LP and just west of Lanzarote, that constitutive the EB, has the same variability. The seasonal cycle of the EB is in agreement with the seasonal cycle of the AMOC that requires the smallest contribution for the T_{UMO} to be in fall, since the AMOC has its maximum northward transport in fall.

Once the seasonal cycle of the ocean circulation in the Canary basin has been described, and validated using different data sets, it is natural to ask the role that Rossby waves play in explaining it, since *Kanzow et al.* [2010] explained 4.3 Sv of the seasonal cycle of the AMOC using a linear Rossby wave model. The results of these authors imply that the seasonal variation of T_{UMO} is almost entirely attributable to changes in stratification at the eastern boundary caused by local wind stress curl variations.

Using the same model of a linear, subinertial response of a stratified ocean to wind stress curl variability as in *Kanzow et al.* [2010], and after separating the linearized equations for a stratified ocean into vertical

modes, the pressure is described by $p(x,y,z,t) = p_n(x,y,x) \cdot F_n(z)$, and the response of the pressure for the low-frequency, large-scale wind forcing is

$$\frac{\partial p_n}{\partial t} - \gamma_n \frac{\partial p_n}{\partial x} = B_n \cdot \nabla \times \tau \qquad (4)$$

where c_n is the nth vertical mode long gravity wave speed and $\gamma_n = \frac{\beta c_n^2}{f}$ is the long Rossby wave speed for the nth vertical mode, and the projection of the forcing onto the vertical mode is scaled with

$$B_n = -\frac{c_n^2}{fH_{mix}} \frac{\int_{-H_{mix}}^0 F_n(z)dz}{\int_{-H}^0 F_n^2(z)dz} \qquad (5)$$

Equations (4) and (5) can be solved in a forward time-stepping mode from zero initial conditions using the climatological seasonal cycle of the wind stress curl (WSC) anomaly across 26.5°N (Figure 13a) obtained from the Scatterometer Climatology of Ocean Winds (SCOW). The equilibrium seasonal cycle of p_n across the basin then results in a basin wide mid-ocean geostrophic transport anomaly for each mode, of

$$T_n^{RW}(z) = \int_{West}^{East} v_n(z)dz = \int_{West}^{East} \frac{1}{\rho f_0} \frac{\partial p_n}{\partial x} \phi_n(z)dx =$$
$$\frac{1}{\rho f_0} \phi_n(z)[p_n(x_{East}) - p_n(x_{west})] \qquad (6)$$

where the seasonal cycle of $p_n(x_{East})$ is the solution at the eastern boundary, while the western boundary signal $p_n(x_{West})$ takes into account the solution at the western boundary and the accumulated effects of Rossby wave propagation from the east. The corresponding meridional overturning transport would be $\Psi_{max}^{RW} = \int_{H_{max}}^0 T_n^{RW}(z)dz$, where h_{max} was chosen to be the depth of the lower boundary of the upper ocean northward-flowing branch of the AMOC.

The simulated seasonal cycle of the meridional overturning transport for the first two modes, with H_{min} = 100 m, H_{max} above the zero level (=950 m), Rossby wave speeds of γ_1 = 4.3 cm s^{-1} and γ_2 = 0.8 cm s^{-1} and SCOW stress curl at 26.5°N across the Atlantic until 16.125°W (Figure 13a), has an amplitude of 5.5 Sv. This amplitude is very similar to the simulation obtained by *Kanzow et al.* [2010]. Also the simulation suggests that the response is mostly due to pressure changes at the eastern boundary, since the contribution from the western boundary is small (Figure 13b).

To understand the sensitivity of the simulated seasonal cycle of the meridional overturning transport to slight changes in the different parameters of the model, and therefore assess the robustness of the Rossby wave model in explaining the seasonal cycle of the AMOC, we performed different simulations where we modified the Rossby wave speed for the first vertical mode and the wind stress curl anomaly.

In the first set of tests, we used a Rossby wave speed for the first two vertical modes of $\gamma_1 = \gamma_2 = 0$ cm s^{-1}. A zero velocity means that Rossby waves do not propagate and therefore the observed changes at the western and eastern boundaries are only consequences of the local forcing. In these simulations (Figure 13b), the seasonal cycle of the meridional overturning transport is very similar to the previous simulations, with a seasonal cycle of around 5.0 Sv indicating that, at least in this model, Rossby waves do not contribute significantly to the simulated seasonal cycle. To understand these results, we did several further simulations where we slightly changed the position of the eastern boundary, and therefore the wind stress curl anomaly that forced the model. Since the SCOW data set has a 0.25° resolution, we performed three simulations where we chose the eastern boundary to be one grid point east and one grid point west of the original simulations performed by *Kanzow et al.* [2010]. We also did one additional simulation where we chose the eastern boundary to be at the easternmost grid point provided by SCOW.

In the simulation where the eastern boundary was moved one grid point (0.25°) west and, therefore, where SCOW stress curl anomaly forced the model right across the Atlantic to 16.375°W (Figure 13c), the simulated seasonal cycle of the meridional overturning has an amplitude of only 3.0 Sv, with the maximum in November and the minimum in June. If the wind stress curls anomaly forcing the model is integrated one grid point (0.25°) east of the *Kanzow et al.* [2010] simulations, the simulated seasonal cycle of the meridional overturning has an amplitude of 6.2Sv. If the integrations are performed using all the data in SCOW up to
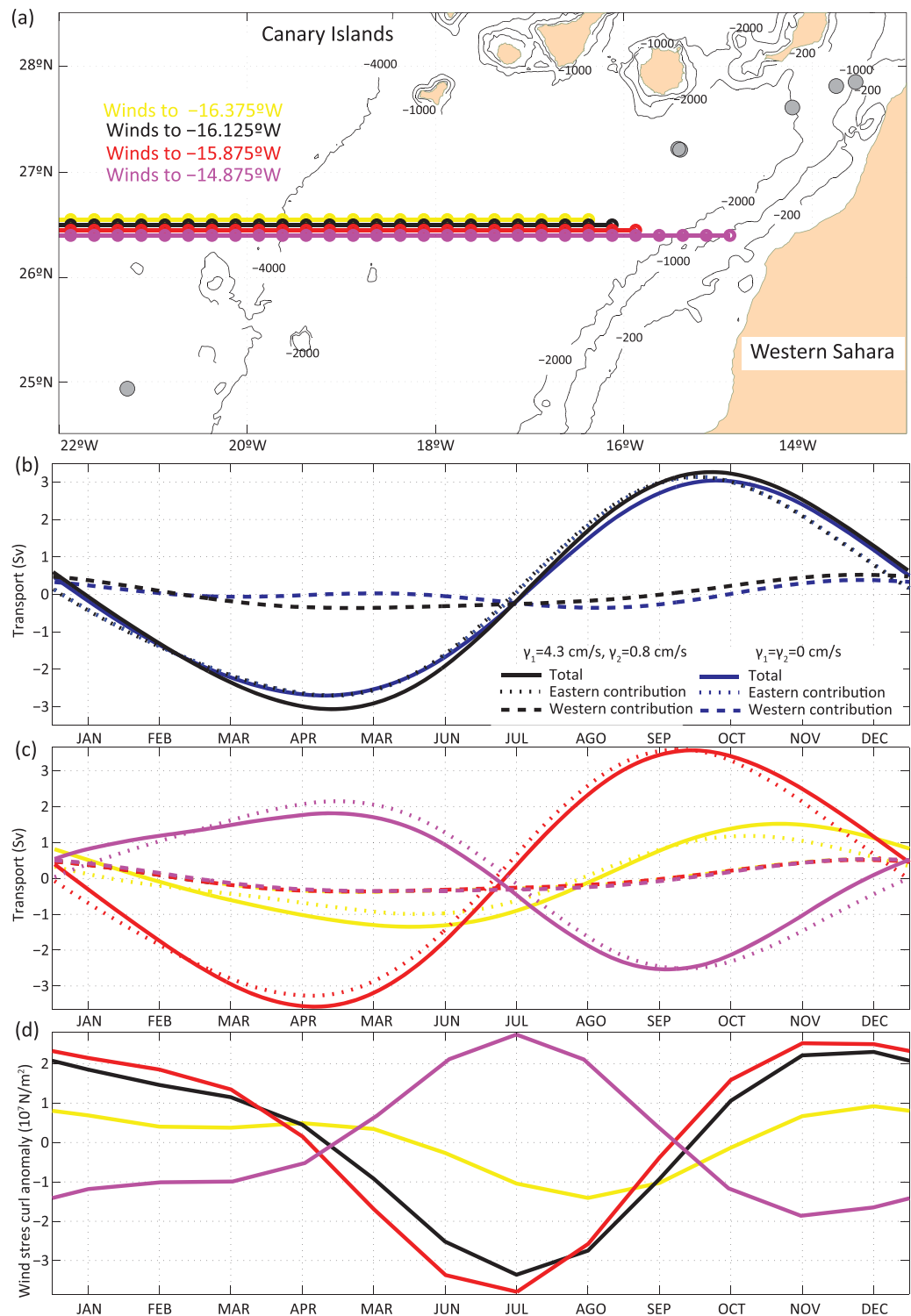
Figure 13. Results from the Rossby wave model. (a) Map of the area with colored lines indicating the SCOW stress curl anomaly used in the integration of the Rossby wave model. Each simulation had a different range of SCOW stress curl anomaly, and the numbers indicate the eastern limits of the wind stress curls that were used. (b) Mid-ocean transport from the Rossby wave model obtained with the first two modes and using SCOW stress curl anomaly to 16.125°W. (c) Same as Figure 13b but using SCOW stress curl anomaly to 16.375°W, 15.875°W, and 14.875°W. The color code is the same as in Figure 13a. (d) SCOW wind stress curl anomaly extracted at 26.5°N for the different winds stress curls used. The color code is the same as in Figure 13a.

the African coastline, i.e., 14.87°W, the simulated seasonal cycle of the meridional overturning has an amplitude of −3.8 Sv, i.e., of opposite sign, with the minimum in fall and the maximum in spring (Figure 13d). From the results of these simulations, it seems that the model used here, that is the same as used by *Kanzow et al.* [2010], is not appropriate to simulate the seasonal cycle of the meridional overturning due to its high sensitivity to small changes in the winds that force the model. The reason that the model is not appropriate is because the geostrophic approach is used to obtain the basin wide mid-ocean transport from p_n across the basin in equation (6), as done by *Kanzow et al.* [2010]. The wind forcing should be coherent with the geostrophic approach and its associated scales. In agreement with this statement, simulations (not shown) where the wind forcing is smoothed using a 50 km low pass filter, or where NCEP winds are used, yield amplitudes for the seasonal cycle of the meridional overturning of only 0.5 Sv, coherent with previous studies that did not find important the role of Rossby waves in determining the seasonality of the AMOC [*Bryan*, 1982; *Böning et al.*, 1994; *Jayne and Marotzke*, 2001], and with observations from the RAPID-MOCHA array that did not found Rossby waves propagating westward [*Chidichimo et al.*, 2010; *Szuts et al.*, 2012]. *Sturges and Hong* [1995] and *Zhang and Wu* [2010] found important the role of the Rossby waves in explaining interannual and decadal variability of sea level and sea surface temperature in the North Atlantic, but not, for the seasonal variability. Additionally, recent results have found that the seasonal variability of the AMOC at 26.5°N is due to the redistribution of water mass, driven by both, local and remote wind stress forcing [*Yang*, 2015].

If Rossby waves cannot explain the seasonal cycle of the CC and the circulation at the EB, and both sides of Lanzarote, a different dynamical forcing has to be proposed. In the oceanic region, the Sverdrup wind-driven circulation has been demonstrated to explain the seasonal cycle in the region [*Fraile-Nuez and Hernández-Guerra*, 2006]. However, east of 15°W, the Sverdrup wind-driven circulation does not explain the seasonal cycle [*Machín et al.*, 2010]. It has been speculated that the flow in the LP is due to the upwelling off northwest Africa, the CUC, the upwelling jet that originates in the upwelling front [*Pelegrí et al.*, 2005; *Mason et al.*, 2011]. However, both during spring (0.7 ± 0.2 Sv) and fall (0.4 ± 0.3 Sv), the net mass transport for the shallowest two layers, that correspond to the thermal front, were low and therefore the total associated seasonal cycle was only −0.3 ± 0.1 Sv. With this low seasonal cycle, we can conclude that the northward flow through the LP in fall has a minor relation to the upwelling, as suggested by *Mason et al.* [2011] and *Pérez-Hernández et al.* [2015]. Since altimetry is representative of the surface flow, it is clear that the flow of the SW in the LP is a recirculation of the CC and not the CUC.

Pérez-Hernández et al. [2015] found a significant correlation between the seasonal cycle of mass transport in the LP and the upper mid-ocean transport in the Atlantic measured by the RAPID-MOCHA array. Using the mean seasonal cycle, computed with EBC4 data between 1997 and 2010, these authors found a correlation of 0.75 for the transport of the NACW measured by the EBC4 mooring at zero lag, and 0.77/0.85, respectively, at 1 month lag for the transport of AAIW/MW. This 1 month lag indicates that the reversal at the intermediate level found in the LP is detected first in the RAPID-MOCHA array, while the surface reversal occurs at the same time in the RAPID-MOCHA array and in the EBC4 mooring. As pointed by the authors, this suggests two separate driving mechanisms for the northward surface and intermediate flow observed in fall at the LP. For the SW and NACW, the mechanism suggested by the authors is the recirculation of the CC, probably forced by the giant filament off Cape Ghir [*Pelegrí et al.*, 2005], coherent with our results. As described previously, this reversal contributes significantly to the seasonal cycle of the SW and NACW during fall. For the intermediate waters, several authors [*Fraile-Nuez et al.*, 2010; *Machín et al.*, 2010] found that the flow of the Canary Intermediate Poleward Undercurrent (IPUC) reverses in the LP, flowing northward during fall. However, all these studies were carried out using data from the EBC4 mooring in the LP, and therefore did not have any information about the flow west of Lanzarote, that we have demonstrated to be similar to the flow in the LP, making the seasonal cycle higher than if just the LP were considered. Although *Machín et al.* [2010] attributed the northward flow during fall in the LP to isopycnal stretching due to wind forcing, we have found a northward flow on both sides of Lanzarote, as suggested by *Barton* [1989], who observed that the poleward flow of the eastern boundary of the Atlantic runs from Cape Blanco to the strait of Gibraltar, and pointed out that this flow could be diverted by the presence of the eastern islands of the Canary Island archipelago. Poleward flows are characteristic of eastern boundary margins, and the joint effect of baroclinicity and relief (JEBAR) [*Huthnance*, 1984] has been widely accepted as a main driver of the poleward flows at these boundaries [*Collins et al.*, 2004; *Connolly et al.*, 2014]. The diversion of the poleward flow by the

presence of the eastern islands of the Canary Island archipelago is a plausible hypothesis since the JEBAR effect is a consequence of the baroclinicity of the flow, and its interaction with the topography of the eastern margin of the ocean, that in the case of the subtropical Atlantic includes the coast of Africa and also the coast of Lanzarote, due to its proximity to the African coast. This would explain the large transport found west of Lanzarote that can be considered part of the IPUC. The difference in the observed variability of the CC in the oceanic region and the EB is due to different forcing mechanisms and therefore to the different dynamics in each area.

5. Conclusions

In summary, we have shown that there is an intense seasonal cycle south of the Canary Islands. The seasonal cycle, defined as Transport$_{Fall}$-Transport$_{Spring}$, for the CC west of 15°W is -4.1 ± 0.5 Sv for the surface, central and intermediate waters. In the region east of 15°W, that we have denominated EB, the seasonal cycle is $+3.7 \pm 0.4$ Sv. This seasonal cycle is in agreement with the seasonal cycle of the AMOC that requires the smallest contribution to the T_{UMO} to be in fall since the AMOC has its maximum northward transport in fall. The seasonal cycle of the EB cannot be explained by a Rossby wave model, since we have demonstrated that the Rossby wave model used by *Kanzow et al.* [2010] is extremely sensitive to the choice of the zonal range of the WSC data and reproduces the same results for a Rossby wave speed of zero. We have also demonstrated that the seasonal cycle of the EB is due, at the central and surface waters, to the recirculation of the Canary Current and, at intermediate levels, to the seasonal cycle of the IPUC, the poleward flow that characterizes the eastern boundaries of the oceans and that, in the case of the Canary Islands, flows through the Lanzarote passage and west of Lanzarote.

References

Barton, E. D. (1989), The poleward undercurrent on the eastern boundary of the subtropical North Atlantic, in *Poleward Flows Along Eastern Ocean Boundaries, Coastal and Estuarine Studies*, vol. 34, edited by S. Neshyba and R. L. Smith, pp. 82–95, Springer, New York.

Böning, C. W., P. Herrmann, and C. W. Böning (1994), Annual cycle of poleward heat transport in the ocean: Results from high-resolution modeling of the North and equatorial Atlantic, *J. Phys. Oceanogr.*, *24*(1), 91–107, doi:10.1175/1520-0485(1994)024.

Bryan, K. (1982), Seasonal variation in meridional overturning and poleward heat transport in the Atlantic and Pacific Oceans: A model study, *J. Mar. Res.*, *40*, 39–53.

Chidichimo, M. P., T. Kanzow, S. A. Cunningham, W. E. Johns, and J. Marotzke (2010), The contribution of eastern-boundary density variations to the Atlantic Meridional Overturning Circulation at 26.5°N, *Ocean Sci.*, *6*(2), 475–490, doi:10.5194/os-6-475-2010.

Collins, C. A., L. M. Ivanov, O. V. Melnichenko, and N. Garfield (2004), California Undercurrent variability and eddy transport estimated from RAFOS float observations, *J. Geophys. Res.*, *109*, C05028, doi:10.1029/96GL02138.

Comas-Rodríguez, I., A. Hernández-Guerra, and E. L. McDonagh (2010), Referencing geostrophic velocities using ADCP data referencing geostrophic velocities using ADCP data, *Sci. Mar.*, *74*(2), 331–338, doi:10.3989/scimar.2010.74n2331.

Connolly, T. P., B. M. Hickey, I. Shulman, and R. E. Thomson (2014), Coastal trapped waves, alongshore pressure gradients, and the California Undercurrent, *J. Phys. Oceanogr.*, *44*(1), 319–342, doi:10.1175/JPO-D-13-095.1.

Cunningham, S. A., et al. (2007), Temporal variability of the Atlantic Meridional Overturning Circulation at 26.5°N, *Science*, *317*(5840), 935–938, doi:10.1126/science.1141304.

Fischer, J., and M. Visbeck (1993), Deep velocity profiling with self-contained ADCPs, *J. Atmos. Oceanic Technol.*, *10*(5), 764–773, doi:10.1175/1520-0426(1993)010.

Fraile-Nuez, E., and A. Hernández-Guerra (2006), Wind-driven circulation for the eastern North Atlantic Subtropical Gyre from Argo data, *Geophys. Res. Lett.*, *33*, L03601, doi:10.1029/2005GL025122.

Fraile-Nuez, E., F. Machín, P. Vélez-Belchí, F. López-Laatzen, V. Benítez-Barrios, and A. Hernández-Guerra (2010), Nine years of mass transport data in the eastern boundary of the North Atlantic Subtropical Gyre, *J. Geophys. Res.*, *115*, C09009, doi:10.1029/2010JC006161.

Ganachaud, A. (2003), Large-scale mass transports, water mass formation, and diffusivities estimated from World Ocean Circulation Experiment (WOCE) hydrographic data, *J. Geophys. Res.*, *108*(C7), 3213, doi:10.1029/2002JC001565.

Hernández-Guerra, A., and L. D. Talley (2016), Meridional overturning transports at 30°S in the Indian and Pacific Oceans in 2002–2003 and 2009, *Prog. Oceanogr.*, *146*, 89–120, doi:10.1016/j.pocean.2016.06.005.

Hernández-Guerra, A., J. Arístegui, M. Cantón, and L. Nykjaer (1993), Phytoplankton pigment patterns in the Canary Islands area as determined using Coastal Zone Colour Scanner data, *Int. J. Remote Sens.*, *14*(7), 1431–1437, doi:10.1080/01431169308953977.

Hernández-Guerra, A., F. López-Laatzen, F. Machín, D. De Armas, and J. L. Pelegrí (2001), Water masses, circulation and transport in the eastern boundary current of the North Atlantic Subtropical Gyre, *Sci. Mar.*, *65*(S1), 177–186, doi:10.3989/scimar.2001.65s1177.

Hernández-Guerra, A., E. Fraile-Nuez, R. Borges, F. López-Laatzen, P. Vélez-Belchí, G. Parrilla, and T. Muller (2003), Transport variability in the Lanzarote passage (eastern boundary current of the North Atlantic subtropical Gyre), *Deep Sea Res., Part I*, *50*(2), 189–200, doi:10.1016/S0967-0637(02)00163-2.

Hernández-Guerra, A., E. Fraile-Nuez, F. López-Laatzen, A. Martínez, G. Parrilla, and P. Vélez-Belchí (2005), Canary Current and North Equatorial Current from an inverse box model, *J. Geophys. Res.*, *110*, C12019, doi:10.1029/2005JC003032.

Hernández-Guerra, A., J. L. Pelegrí, E. Fraile-Nuez, V. Benítez-Barrios, M. Emelianov, M. D. Pérez-Hernández, and P. Vélez-Belchí (2014), Meridional overturning transports at 7.5 N and 24.5 N in the Atlantic Ocean during 1992–93 and 2010–11, *Prog. Oceanogr.*, *128*, 98–114, doi:10.1016/j.pocean.2014.08.016.

Huthnance, J. M. (1984), Slope currents and ''JEBAR,'' *J. Phys. Oceanogr.*, *14*, 795–810.

Jayne, S. R., and J. Marotzke (2001), The dynamics of ocean heat transport variability, *Rev. Geophys.*, *39*(3), 385–411, doi:10.1029/2000RG000084.

Kanzow, T., S. A. Cunningham, D. Rayner, J. J. M. Hirschi, W. E. Johns, M. O. Baringer, H. L. Bryden, L. M. Beal, C. S. Meinen, and J. Marotzke (2007), Observed flow compensation associated with the MOC at 26.5°N in the Atlantic, *Science*, *317*(5840), 938–941, doi:10.1126/science.1141293.

Kanzow, T., et al. (2010), Seasonal variability of the Atlantic Meridional Overturning Circulation at 26.5°N, *J. Clim.*, *23*(21), 5678–5698, doi:10.1175/2010JCLI3389.1.

Laiz, I., J. L. Pelegrí, F. Machín, P. Sangra, A. Hernández-Guerra, A. Marrero-Díaz, and A. Rodríguez-Santana (2012), Eastern boundary drainage of the North Atlantic Subtropical Gyre, *Ocean Dyn.*, *62*(9), 1287–1310, doi:10.1007/s10236-012-0560-6.

Machín, F., A. Hernández-Guerra, and J. L. Pelegrí (2006), Mass fluxes in the Canary Basin, *Prog. Oceanogr.*, *70*(2–4), 416–447, doi:10.1016/j.pocean.2006.03.019.

Machín, F., J. L. Pelegrí, and E. Fraile-Nuez (2010), Seasonal flow reversals of Intermediate Waters in the Canary Current System east of the Canary Islands, *J. Phys. Oceanogr.*, *40*(8), 1902–1909, doi:10.1175/2010JPO4320.1.

Mason, E., F. Colas, J. Molemaker, A. F. Shchepetkin, C. Troupin, J. C. McWilliams, and P. Sangra (2011), Seasonal variability of the Canary Current: A numerical study, *J. Geophys. Res.*, *116*, C06001, doi:10.1029/2010JC006665.

McCarthy, G. D., D. A. Smeed, and W. E. Johns (2015), Measuring the Atlantic Meridional Overturning Circulation at 26°N, *Prog. Oceanogr.*, *130*, 91–111, doi:10.1016/j.pocean.2014.10.006.

Pacheco, M. M., and A. Hernández-Guerra (1999), Seasonal variability of recurrent phytoplankton pigment patterns in the Canary Islands area, *Int. J. Remote Sens.*, *20*(7), 1405–1418, doi:10.1080/014311699212795.

Pelegrí, J. L., J. Arístegui, A. Hernández-Guerra, S. Hernández-León, A. Marrero-Díaz, M. F. Montero, and P. Sangrà (2005), Coupling between the open ocean and the coastal upwelling region off northwest Africa: Water recirculation and offshore pumping of organic matter, *J. Mar. Syst.*, *54*(1–4), 3–37, doi:10.1016/j.jmarsys.2004.07.003.

Pérez-Hernández, M. D., A. Hernández-Guerra, E. Fraile-Nuez, I. Comas-Rodríguez, V. M. Benítez-Barrios, J. F. Domínguez-Yanes, P. Vélez-Belchí, and D. De Armas (2013), The source of the Canary Current in fall 2009, *J. Geophys. Res. Oceans*, *118*, 2874–2891, doi:10.1002/jgrc.20227.

Pérez-Hernández, M. D., G. D. McCarthy, P. Vélez-Belchí, D. A. Smeed, E. Fraile-Nuez, and A. Hernández-Guerra (2015), The Canary Basin contribution to the seasonal cycle of the Atlantic Meridional Overturning Circulation at 26°N, *J. Geophys. Res. Oceans*, *120*, 7237–7252, doi:10.1002/2015JC010969.

Ruiz, S., J. L. Pelegrí, M. Emelianov, A. Pascual, and E. Mason (2014), Geostrophic and ageostrophic circulation of a shallow anticyclonic eddy off Cape Bojador, *J. Geophys. Res. Oceans*, *119*, 1257–1270, doi:10.1002/2013JC009169.

Stramma, L. (1984), Geostrophic transport in the Warm Water Sphere of the eastern subtropical North Atlantic, *J. Mar. Res.*, *42*(3), 537–558, doi:10.1357/002224084788506022.

Stramma, L., and T. J. Müller (1989), Some observations of the Azores Current and the North Equatorial Current, *J. Geophys. Res.*, *94*(C3), 3181–3186, doi:10.1029/JC094iC03p03181.

Stramma, L., and G. Siedler (1988), Seasonal changes in the North Atlantic Subtropical Gyre, *J. Geophys. Res.*, *93*(C7), 8111–8118, doi:10.1029/JC093iC07p08111.

Sturges, W., and B. G. Hong (1995), Wind forcing of the Atlantic thermocline along 32°N at low frequencies, *J. Phys. Oceanogr.*, *25*(7), 1706–1715, doi:10.1175/1520-0485(1995)025<1706:WFOTAT>2.0.CO;2.

Szuts, Z. B., J. R. Blundell, M. P. Chidichimo, and J. Marotzke (2012), A vertical-mode decomposition to investigate low-frequency internal motion across the Atlantic at 26°N, *Ocean Sci.*, *8*(3), 345–367, doi:10.5194/os-8-345-2012.

Tel, E., et al. (2016), IEOOS: The Spanish Institute of Oceanography Observing System, *Ocean Sci.*, *12*(2), 345–353, doi:10.5194/os-12-345-2016.

Vélez-Belchí, P., L. R. Centurioni, D.-K. Lee, S. Jan, and P. P. Niiler (2013), Eddy induced Kuroshio intrusions onto the continental shelf of the East China Sea, *J. Mar. Res.*, *71*(1–2), 83–107.

Vélez-Belchí, P., M. González-Carballo, M. D. Pérez-Hernández, and A. Hernández-Guerra (2015), Open ocean temperature and salinity trends in the Canary Current Large Marine Ecosystem, in *Oceanographic and Biological Features in the Canary Current Large Marine Ecosystem, IOC Tech. Ser. 115*, edited by L. Valdés and I. Déniz-González, pp. 299–308, IOC-UNESCO, Paris.

Yang, J. (2015), Local and remote wind stress forcing of the seasonal variability of the Atlantic Meridional Overturning Circulation (AMOC) transport at 26.5°N, *J. Geophys. Res. Oceans*, *120*, 2488–2503, doi:10.1002/2014JC010317.

Zhang, H., and L. Wu (2010), Predicting North Atlantic sea surface temperature variability on the basis of the first-mode baroclinic Rossby wave model, *J. Geophys. Res.*, *115*, C09030, doi:10.1029/2009JC006017.

Zhao, J., and W. Johns (2014), Wind-driven seasonal cycle of the Atlantic Meridional Overturning Circulation, *J. Phys. Oceanogr.*, *44*(6), 1541–1562, doi:10.1175/JPO-D-13-0144.1.